



The MILAN campaign: Studying diel light effects on the air-sea interface

Christian Stolle^{1, 2, *, #}, Mariana Ribas-Ribas^{2, #}, Thomas H. Badewien², Jonathan Barnes³, Lucy J. Carpenter⁴, Rosie Chance⁴, Lars Riis Damgaard⁵, Ana María Durán Quesada^{6, 7}, Anja Engel⁸, Sanja Frka⁹, Luisa Galgani¹⁰, Blaženka Gašparović⁹, Michaela Gerriets², Nur Ili Hamizah Mustaffa^{2, 11}, Hartmut Herrmann¹², Liisa Kallajoki¹¹, Ryan Pereira¹³, Franziska Radach¹, Niels Peter Revsbech⁵, Philippa Rickard³, Adam Saint⁴, Matthew Salter¹⁴, Maren Striebel¹¹, Nadja Triesch¹², Guenther Uher³, Robert C. Upstill-Goddard³, Manuela van Pinxteren¹², Birthe Zäncker⁸, Paul Zieger¹⁴, Oliver Wurl²

*corresponding author: christian.stolle2@uni-oldenburg.de

both authors contributed equally to the work

¹ Leibniz-Institute for Baltic Sea Research Warnemuende, 18119 Rostock, Germany

² Center for Marine Sensors, Institute for Chemistry and Biology of the Marine Environment, Carl-von-Ossietzky University Oldenburg, 26382 Wilhelmshaven, Germany

³ School of Natural and Environmental Sciences, Newcastle University, NE1 7RU, Newcastle, United Kingdom

⁴ Wolfson Atmospheric Chemistry Laboratories, Department of Chemistry, University of York, YO10 5DD, York, United Kingdom

⁵ WATEC, Department of Bioscience, Aarhus University, 8000 Aarhus, Denmark

⁶ Atmospheric, Oceanic and Planetary Physics Department, School of Physics, University of Costa Rica, 11501 San José, Costa Rica

⁷ Center for Geophysical Research, University of Costa Rica, 11501 San José, Costa Rica

⁸ GEOMAR Helmholtz Centre for Ocean Research Kiel, 24105 Kiel, Germany

⁹ Division for Marine and Environmental Research, Rudjer Boskovic Institute, 10000 Zagreb, Croatia

¹⁰ Environmental Spectroscopy Group, DBCF, University of Siena, 53100 Siena, Italy

¹¹ Institute for Chemistry and Biology of the Marine Environment, Carl-von-Ossietzky University Oldenburg, 26382 Wilhelmshaven, Germany

¹² Leibniz-Institute for Tropospheric Research (TROPOS), Atmospheric Chemistry Department (ACD) 04318 Leipzig, Germany

¹³ Lyell Centre, Heriot-Watt University, EH14 4AP, Edinburgh, United Kingdom

¹⁴ Department Environmental Science and Analytical Chemistry & Bolin Centre for Climate Research, Stockholm University, 11418 Stockholm, Sweden

Early Online Release: This preliminary version has been accepted for publication in *Bulletin of the American Meteorological Society*, may be fully cited, and has been assigned DOI 10.1175/BAMS-D-17-0329.1. The final typeset copyedited article will replace the EOR at the above DOI when it is published.

ABSTRACT

The sea-surface microlayer (SML) at the air-sea interface is < 1 mm deep but it is physically, chemically and biologically distinct from the underlying water and the atmosphere above. Wind-driven turbulence and solar radiation are important drivers of SML physical and biogeochemical properties. Given that the SML is involved in all ocean-atmosphere exchanges of mass and energy, its response to solar radiation, especially in relation to how it regulates the air-sea exchange of climate-relevant gases and aerosols, is surprisingly poorly characterised.

MILAN (sea-surface *MicroLayer* at Night) was an international, multidisciplinary campaign designed to specifically address this issue. In spring 2017, we deployed diverse sampling platforms (research vessels, radio-controlled catamaran, free-drifting buoy) to study full diel cycles in the coastal North Sea SML and in underlying water, and installed a land-based aerosol sampler. We also carried out concurrent ex situ experiments using several microsenors, a laboratory gas exchange tank, a solar simulator, and a sea spray simulation chamber.

In this paper we outline the diversity of approaches employed and some initial results obtained during MILAN. Our observations of diel SML variability, e.g. the influence of changing solar radiation on the quantity and quality of organic material, and diel changes in wind intensity primarily forcing air-sea CO₂ exchange, underline the value and the need of multidisciplinary campaigns for integrating SML complexity into the context of air-sea interaction.

56 **CAPSULE**

57 MILAN was a multidisciplinary, international study examining how the diel
58 variability of sea-surface microlayer biogeochemical properties potentially impacts ocean-
59 atmosphere interaction, in order to improve our understanding of this globally important
60 process.

61

BACKGROUND

The sea-surface microlayer (SML) occupies the uppermost tens to hundreds of μm of the ocean surface and is ubiquitous (Wurl et al. 2011). Consequently, it is in direct contact with the atmosphere and covers around 70% of Earth's surface. Compared to the underlying bulk water, the SML is characterised by distinct biological and physicochemical properties (Cunliffe et al. 2013), which is important given that all ocean-atmosphere exchanges of mass and energy must necessarily cross it. An improved understanding of the SML is thus essential for studying air-sea exchange processes that have important implications for global biogeochemical cycles, climate regulation, and air quality (Wurl et al. 2017).

The SML experiences instantaneous meteorological forcing by e.g., solar radiation, wind and precipitation. Solar radiation directly influences the thermal and saline boundary layer with variable thicknesses in the order of 1000 μm (Saunders 1967) and 200 μm (Katsaros 1980), respectively. Evaporation and precipitation have a strong influence on the thermal and saline properties of the SML (Schlüssel et al. 1997). Furthermore, recent measurements show that large enrichment of organic material in the SML reduces evaporation from the sea-surface (Wurl et al. 2018). The SML also experiences higher exposure to UV radiation than does the underlying water column, because light attenuation by optically active components and water itself reduce light levels exponentially with increasing depth. Whereas light levels in the SML always exceed 98% of surface irradiance, in coastal environments with large amounts of suspended and dissolved organic matter only around 10% of surface UV-B irradiance may reach 0.2 to 5 m depth (Smyth 2011; Tedetti and Sempéré 2006).

Wind induced formation of small capillary waves, and microscale breaking causes SML disruption (Ocampo-Torres et al. 1994). After disruption, re-establishment of the thermal skin layer occurs (Jessup et al. 2009) and depends on wind speed. Re-establishment occurs on a timescale of between several seconds and around one minute, the latter being

typical in the absence of wind (Jessup et al. 1995; Mobasheri 2006). If wind stress continues, larger waves form and break, promoting the turbulent mixing of near-surface water (Farmer et al. 1993). Wave breaking entrains air into the water column, forming air bubbles that rise upwards to the SML where they eventually burst. This process concentrates material within the SML (Robinson et al. 2019; Zhou et al. 1998) and causes rapid reformation of the SML within seconds (Cunliffe et al. 2013). However, for a certain fraction of the material, bubble bursting is also an important route from the underlying bulk water via the SML into the atmosphere (Memery and Merlivat 1985). Sea spray aerosols arising from bubble bursting may act as cloud condensation nuclei, supporting the growth of low-level clouds (Latham et al. 2008) that impact ocean surface temperatures (Tanimoto and Xie 2002) and radiation fluxes (Bunker 1976; Curry and Ebert 1992) and, in consequence, the Earth's energy budget (Watanabe et al. 2018). Sea spray aerosols are a complex mixture of sea salt, organic material and microorganisms (Bigg and Leck 2008; Quinn et al. 2015). Organic material in the SML shows strong ice-nucleating activity (Wilson et al. 2015), which impacts atmospheric properties, e.g. cloud lifetime (Murray et al. 2012). The SML may additionally influence the formation of secondary organic aerosols via the photochemically induced volatilization of dissolved organics (Alpert et al. 2017; Ciuraru et al. 2015) and is a source of atmospheric iodine via reaction of dissolved iodide with atmospheric ozone (Carpenter et al. 2013).

The SML controls air-sea gas exchange by acting as a diffusive boundary layer (Broecker and Peng 1974; Jähne 2009). According to classical gas exchange theory, the SML resembles a stagnant layer under low winds, when diffusion is the driving force for air-sea gas exchange. In the natural environment this theoretical stagnant layer does not hold true as microscale breaking and buoyancy fluxes occur. Increasing wind speed causes periodic, or at high wind speeds ($> 10 \text{ m s}^{-1}$) probably permanent, SML disruption, and at some point turbulent mixing controls air-sea gas exchange. Parameterizations for gas transfer velocities

solely based on wind speed cannot fully account for in situ observations (Asher 2009; Ribas-
Ribas et al. 2018a; Wanninkhof 2014). For example, CO₂ air-sea fluxes derived from wind-
speed based parameterisations typically have around two-fold uncertainty (Wanninkhof 2014)
due to other controlling variables, including surface-active organic material, bubbles, fetch,
rain, and chemical enhancement, that affect the air-sea gas exchange of climate-relevant gases
(Wanninkhof et al. 2009).

Organic matter in natural waters is a complex mixture of substances, and material
accumulating in the SML includes organic gel particles (Wurl and Holmes 2008),
polysaccharides (Sieburth et al. 1976), lipid-like material (Gašparović et al. 1998; Kattner and
Brockmann 1978), amino acids (Kuznetsova et al. 2004) and Chromophoric Dissolved
Organic Matter (CDOM) (Tilstone et al. 2010). The tendency is for many of these
components to be of lower molecular weight than their analogues in the underlying water
(Lechtenfeld et al. 2013). This may be coupled to in situ primary production (Chin et al. 1998;
Passow 2002), allochthonous inputs of terrestrial material of either natural (e.g. Frew et al.
(2006)) or anthropogenic (Guitart et al. 2007) origin, and the photochemical and/or microbial
reworking of higher molecular weight material (Schulz et al. 2013; Tilstone et al. 2010).

Many of the organic substances in the SML have a particularly high interfacial
affinity, so are often called Surface Active Substances (SAS) or surfactants. Surfactants in the
SML are of mostly biological origin, e.g. phytoplankton exudates (Žutić et al. 1981), material
released during zooplankton grazing (Kujawinski et al. 2002) and bacterial by-products
(Satpute et al. 2010). In coastal waters there may be additional surfactant contributions from
terrestrial sources (Pereira et al. 2016). Surfactants accumulate in the SML via diffusion at
low wind or bubble scavenging at moderate to high winds, and have been shown to be present
at wind speeds up to 13 m s⁻¹ (Sabbaghzadeh et al. 2017). Laboratory and field experiments
have shown surfactants to suppress air-sea gas exchange by up to 50% (Frew et al. 1990;

Pereira et al. 2016; Ribas-Ribas et al. 2018b), and that neglecting this effect can greatly overestimate air-sea gas exchange rates (Mustaffa et al. in preparation; Pereira et al. 2018; Salter et al. 2011). In addition, photochemical reactions involving SML organics have the potential to modify surfactant concentrations and compositions, and can produce trace gases directly (Carpenter and Nightingale 2015). Photo-oxidation and dissolution of these and other organic components will feedback on aquatic ecosystems (Häder et al. 2015). For certain atmospheric gases, most notably ground-level ozone (an air pollutant), chemical reactions taking place at the air-sea interface are a significant removal process (e.g. Ganzeveld et al. (2009)).

Under certain conditions, the SML includes complex microbial communities embedded in a gel-matrix leading to its description as a biofilm-like habitat (Wurl et al. 2016). Prominent examples are large cyanobacteria blooms floating at the sea surface (Sieburth and Conover 1965; Wurl et al. 2018). While the SML is a challenging habitat for organisms, especially due to maximal exposure to solar radiation, it nevertheless has an inherently wide microbial diversity that is often distinct from the underlying water (Cunliffe and Murrell 2009; Hardy 1982; Joux et al. 2006; Stolle et al. 2011). Diel patterns in the abundance and activity of several types of organisms ranging from bacteria to phytoplankton and zooplankton close to or in the SML have been reported, presumably reflecting at least in part, a solar radiation response (Carlucci et al. 1986; Holdway and Maddock 1983; Maki and Herwig 1991; Wandschneider 1979).

Note: Please place BOX 1 ('MILAN OBJECTIVES') here.

STUDY AREA

MILAN was conducted from April 3rd-13th 2017 in the Wadden Sea region of the south eastern North Sea (Fig. 2). The Wadden Sea is one of the largest areas of intertidal flats worldwide (area $\sim 10^4$ km²) and is divided into several tidal basins. Phytoplankton dynamics in the Wadden Sea are strongly regulated by nutrients and solar radiation, which give rise to spring blooms between March and May (Colijn and Cadée 2003). It is for this reason that MILAN was planned for early-mid April. The MILAN field site was in Jade Bay, one of the Wadden Sea's largest basins, which is influenced by semi-diurnal tides with a tidal range of up to 3.8 m (Götschenberg and Kahlfeld 2008). A large water volume (4×10^8 m³) flows in and out of Jade Bay during each rising and falling tide (Götschenberg and Kahlfeld 2008). However, direct freshwater discharge is relatively small, such that the usual salinity range is 29-32 (Götschenberg and Kahlfeld 2008), similar to that of offshore waters of the German bight (Otto et al. 1990).

During MILAN we performed several field experiments in Jade Bay (Table 1), including two full diel cycles over 25 hours that we present in this paper: Cycle 01 on April 4th to 5th 2017 and Cycle 03 on April 8th to 9th 2017 (Fig. 2). During each cycle, the radio-controlled catamaran 'S³-Sea Surface Scanner' and at least one of the research vessels 'Senckenberg', 'Otzum', or 'Zephyr' followed a passively drifting CO₂ buoy (Fig. 2). Meteorological conditions, and water current speed and direction throughout the entire water column were recorded continuously from the research vessels, supported by observations from land-based weather stations. Water column physical properties were profiled every hour using sensors for conductivity, temperature and density. S³ is equipped with diverse sensors to measure physicochemical properties (e.g. conductivity, temperature, fluorescent dissolved organic matter) of the SML and from 1 meter water depth, referred to throughout this paper as "underlying water" (ULW) (Ribas-Ribas et al. 2017). S³ additionally collected large volume

water samples (20 L) from the SML and the ULW for subsequent analyses in the laboratory, for laboratory experiments using a gas-exchange tank, a solar simulator, a sea spray simulation chamber, and for microsensor experiments. All technical details regarding field measurements and laboratory analyses can be found in the Supplemental Material.

MEASUREMENT HIGHLIGHTS

Meteorological and hydrological conditions

Precise measurements of meteorological and hydrological conditions are crucial for an understanding of processes in the upper ocean and its interaction with the atmosphere. During MILAN we used two weather stations, i.e. a land-based system on the institute building at the shoreline (Institute for Chemistry and Biology of the Marine Environment), and one system in the field (on the masts of ‘S³’), to measure air temperature, and wind speed and direction. Furthermore, we measured water temperature and salinity in the SML (< 1 m) and in the ULW (= 1 m) using ‘S³’ and from 1.2 – 2.0 m water depth using a CTD (conductivity; temperature; depth) package.

Transitions between low- and high-pressure systems were prevalent during MILAN, influencing the intensity of near surface winds. During Cycle 01, a low pressure system developed (Fig. 3 A), causing wind speed to increase at the end of Cycle 01 (Fig. 4 E). During Cycle 03, higher sea level pressure over the European continent (Fig. 3 B) induced a redistribution of the wind flow causing decreasing wind speeds (Fig. 4 F). Throughout the MILAN campaign low clouds covered between 50% and 70% of the study region (Fig. 3 C, D). Cover by low clouds was less extensive during Cycle 01 than during Cycle 03, where increasing cloudiness caused a rapid decrease in surface radiation after noon (Fig. 4 A, B).

Jade Bay is influenced by strong tidal currents that must be taken account of when considering the meteorological forcing of sea surface properties. The maximum current speed in the surface water layer was higher during ebb tide (approx. 1.2 m s⁻¹ for Cycle 01 and 1.4

m s⁻¹ for Cycle 03) than during flood tide (approx. 1 m s⁻¹) (Fig. 5). The current direction during ebb tides was about 330° and during flood tides about 150°.

The near surface air temperature measured from S³ (T^a_{S3}) during MILAN was mild. Diel cycles of T^a_{S3} showed a maximum air temperature range of about 5 °C (Cycle 03). While these diel differences generally followed the influence of solar radiation (Fig. 4 A, B), land-sea breeze effects, due to our coastal study site, might have caused additionally day/night variation of air temperature. Ongoing analyses of the relation between wind speed and direction, solar radiation and air temperature will unravel the main drivers of diel temperature changes during MILAN. The main day to day variations of air temperature were associated to changes in the mean sea level pressure (Fig. 3 A, B). The water temperature measured with the CTD (T^w_{CTD}) varied by < 1 °C during each cycle, ranging from 8.9 °C to 9.7 °C during Cycle 01 and from 9.7 °C to 10.3 °C during Cycle 03 (Fig. 4). Due to solar heating, temperatures in the SML (T^w_{SML}) and in the ULW (T^w_{ULW}) were higher compared to T^w_{CTD} around noon, and T^w_{SML} and T^w_{ULW} showed similar overall temporal dynamics, with a difference between SML and ULW of about ± 0.5 °C (Fig. 4 C).

Temperature-salinity diagrams constructed from the CTD data revealed very little temporal change during Cycle 03 (Fig. 6). Mean CTD salinity during the day was 32.89 and during the night 32.86, while mean CTD temperature was 9.97 °C during the day and 9.92 °C during the night. The depth of CTD measurements represents the penetrating depth of our free-drifting buoy, consequently our sampling strategy consistently targeted the same water mass. Compared to the CTD, we observed stronger temporal variability of temperature and salinity in the SML and ULW throughout Cycle 03. Salinity ranged from 29.2 to 32.1 in the SML and from 31.7 to 34.4 in the ULW. Temperature ranged from 8.8 to 12.1 in the SML and from 8.6 to 11.0 in the ULW. This contrasting behaviour between measurements from the SML and ULW, as measured by S³, versus measurements from the CTD is deserving of further consideration, especially in relation to how the complex bathymetry of Jade Bay along

with meteorological forcing influences the mixing of saline North Sea water with less saline water of the inner Jade Bay. This significant difference between the SML and ULW implies the presence of two distinct water layers within the uppermost 1 m of the water column.

Light-driven changes in organisms inhabiting the SML

The metabolic activity of organisms, especially of microorganisms, determines the production, degradation, and modification of organic material in the surface ocean (Azam and Malfatti 2007). The underlying processes of primary production and respiration also directly influence the concentration and air-sea fluxes of e.g. CO₂ (Calleja et al. 2005). Primary production by phytoplankton is generally light dependent, but excessive radiation levels may cause inhibition of photosynthesis (van de Poll et al. 2006). During MILAN Cycles 01 and 03 we observed similar diel patterns for the relative concentration (SML versus ULW) of the photosynthetic pigment chlorophyll-*a*, an index of phytoplankton biomass, especially during the first half of both cycles (Fig. 7 A). The relative concentration is expressed as the enrichment factor (EF), i.e. the concentration of a parameter *X* in the SML vs. ULW ($EF = X_{[SML]} / X_{[ULW]}$). Chlorophyll-*a* was generally lower in the SML than in the ULW ($EF < 1$), as reported previously (Falkowska 2001). During both cycles, lowest EFs were observed around noon, and despite large variability in the data collected, these dynamics indicate that SML accumulation of phytoplankton may be radiation dependent (Fig. 7 B). Detailed analyses of specific phytoplankton groups will help in the future to refine previously observed diel, species-specific migration of planktonic organisms (Wandschneider 1979). Preliminary results indicate a radiation-dose dependent accumulation of Cryptophytes in the SML at low levels of solar radiation (Fig. 7 D), even though their diurnal dynamics were very irregular (Fig. 7 C).

Bacteria are integral members of the gelatinous matrix of the SML (Wurl et al. 2016), and their activity and community composition may change due to changing solar radiation

(Santos et al. 2009; Stolle et al. 2011). Bacterial abundance was often higher in the SML than in the ULW and the data contained a temporal signal, particularly during the first half of each cycle (Fig. 7 E) when increased enrichment was evident even at high radiation levels (Fig. 7 F). While these results imply that bacterial enrichment of the SML is not negatively affected by solar radiation, other features of the data need further detailed analyses. For example, the strongest bacterial depletion was at night, when wind speed was very low. While low wind speed usually favors the enrichment of bacteria in the SML (Rahlff et al. 2017), microbial food web interaction in the SML (Joux et al. 2006), e.g. enhanced protist feeding on bacteria during nighttime, is possible.

Diel patterns of organic material in the SML

Dissolved organic matter

Organic matter in natural waters is a complex mixture of molecules and understanding the variability in the composition of the dissolved organic matter (DOM) bulk pool will help to unravel its production and degradation pathways. During Cycle 03, dissolved organic carbon concentrations in the SML and ULW ranged between 2.6-2.8 mg L⁻¹ (Fig. 8 A) without any significant enrichments in the SML compared to the ULW (EF = 0.97-1.05).

The DOM composition also varied little between the SML and the ULW in terms of percentage contribution (Humic Substances, 47-49%; low molecular weight neutrals, 32-34%; Building Blocks, 12-13%; Biopolymers, 6-7%; and low molecular weight acids, 1%; Fig. 8 A). While some variations in SML enrichment were observed across the DOM composition pools (data not shown), a clear description of any diel patterns must await our complete analysis of all the samples collected. Nevertheless, some potential production pathways may be identified, as the enrichment of biopolymers in the SML followed patterns of chlorophyll-*a* enrichment in the SML (Fig. 8 B). Further detailed analyses will unravel which substrate

classes of the DOM pool may be linked to primary or secondary producers, and whether these are influenced by diel radiation signals. Furthermore, while overall DOM composition is very similar in the SML and ULW, the molecular composition may differ strongly (Lechtenfeld et al. 2013). We noted that while the concentration of humic substances remained relatively stable throughout the cycle, the humics nitrogen content was variable over time, suggesting either a change in DOM supply or some reworking of humic substances.

Light absorbance and fluorescence properties of dissolved of organic matter

Chromophoric Dissolved Organic Matter (CDOM) is the light-absorbing fraction of the dissolved organic matter (DOM) pool. CDOM is ubiquitous in coastal and open ocean environments, and often dominates light attenuation in marine waters. CDOM is subject to photochemical and photobiological reactions (Mopper et al. 2015) and is a tracer of deep ocean biogeochemical cycles and circulation (Nelson and Siegel 2013). Marine CDOM can be released by phytoplankton and additionally produced by microbial degradation of DOM (Nelson and Siegel 2013). A fraction of CDOM fluoresces following excitation and is thus referred to as fluorescent Dissolved Organic Matter (fDOM).

CDOM absorbance (measured at a wavelength of 355 nm) in the SML was different between Cycle 01 and 03, both in terms of absolute values and temporal variability (Fig. 9 A). The most obvious difference between the cycles was observed during the night, when either highest (Cycle 01) or lowest (Cycle 03) values were measured. While these patterns currently cannot be easily explained by single forcing factors (e.g. tidal currents, wind speed, solar radiation), we observed that the enrichment of CDOM in the SML tends to be negatively related to radiation intensity (Fig. 9 B). Such changes in CDOM are consistent with CDOM photobleaching (Helms et al. 2008), but further consideration of other important production / degradation mechanisms, e.g. by microorganisms in the SML compared to the ULW, will be needed to elucidate the main driver of CDOM turnover for each cycle studied.

The temporal variability of fDOM in the SML and ULW was very similar throughout Cycle 03, but with generally higher values in the SML (Fig. 9 C). This SML enrichment in fDOM was significantly higher at night (median = 1.57, n = 611) than during daytime (median = 1.38, n = 800) but it was driven by differences in wind speed rather than changes in radiation intensity. During the day, fDOM enrichment was significantly higher at moderate (2.5-5 m s⁻¹) compared to low (0-2.5 m s⁻¹) wind speed, whereas during the night the highest enrichments were observed for low wind speed (Fig. 9 D).

Surfactant dynamics under natural and artificial radiation exposure

Surfactants are organic compounds with strong interfacial affinities that reflect molecular structures. They are adsorbed at the air-sea interface, stabilizing the SML. During MILAN, surfactants in both the SML and the ULW showed characteristics typical of hydrophilic substances, such as humic material, proteins and polysaccharides. We found contrasting temporal dynamics of surfactants in the SML and ULW of Cycle 03 (Fig. 10 A). While ULW surfactant concentration decreased during the night, we observed higher nighttime concentrations of surfactants in the SML, which is significant given that the relative standard deviation of the measurement is < 5% (Supplementary Material). Photochemical production during the night can be excluded and wind-induced turbulent transport was probably minor due to low wind speeds (Fig. 4 F). These observations therefore suggest a strong nighttime biological surfactant production in the SML.

To complement the field studies, we investigated the effect of solar radiation on surfactants in discrete water samples experimentally, using a solar simulator. Surfactants increased during the irradiation of unfiltered SML samples. In the example in Figure 10 B, surfactants in an irradiated SML sample taken during Cycle 03 initially increased by ~9% over the first three hours of irradiation, showing an ~18% increase at 24 hours irradiation. In dark controls, surfactants initially increased by ~4%, showing a 9% increase at 24 hours

incubation. Temperature controls (dark, 4 °C) showed no net change until 24 hours incubation, increasing by ~4%. Temperature controls consistently remained below dark controls, and dark controls below irradiated subsamples.

The observed difference between dark (~20 °C) and temperature (4 °C) controls confirms a temperature effect on surfactant production during laboratory irradiations. Irrespective of this, the larger overall changes in surfactants in the irradiated samples relative to both dark and temperature controls demonstrate a net photochemical production of surfactants during irradiation. Our findings show that photochemical transformations of surfactants should be accounted for when evaluating their enrichment in the SML.

Diel turnover of lipids

Lipids are an important food source to the aquatic food web, because they are carbon-rich and have very high energetic values. Lipids can form a condensed layer at the air-sea interface that can substantially influence material exchange (e.g. of gases) within the marine boundary layer (Gladyshev 2002). Since the molecular structure of lipids determines their reactivity, characterizing marine lipids at the molecular level may help to identify their various sources and the processes responsible for their degradation and transformation (Christodoulou et al. 2009; Van Mooy et al. 2006).

Lipid concentrations in our nutrient rich Jade Bay (Colijn et al. 2002) were much higher compared to oligotrophic regions (Gašparović et al. 2014). Phytoplankton are the main lipid producer in the ocean (Gašparović et al. 2014) and membrane lipids, e.g. glycolipids and phospholipids, were substantial contributors to the lipid pool in our samples. During both cycles, we observed a large variability of particulate lipid concentrations in SML and ULW samples with either higher or lower concentrations occurring in the SML (Fig. 11 A, B). Interestingly, during nighttime of both cycles, we observed higher lipid degradation indices in

the SML compared to the ULW (Fig. 11 C, D). Although confirmation through an analysis of the whole data-set is needed, this preliminary observation indicates that degradation processes likely differ between SML versus ULW and time of day.

Organic gel-like particles

The gelatinous matrix of the SML comprises a complex mixture of inter-tangled molecules and particles. Among the latter, Transparent Exopolymer Particles (TEP) and Coomassie Stainable Particles (CSP) are especially important SML constituents (Galgani et al. 2016; Wurl and Holmes 2008). Increasing accumulation of gel-like particles leads to the formation of a biofilm-like structure in the SML, possibly causing a reduction in gas exchange across the SML (Wurl et al. 2016). During MILAN, CSP concentrations in the SML were on average lower than in the ULW (Fig. 12 A). In contrast, TEP concentrations were not significantly different between SML and ULW (Fig. 12 B), which might be related to overall high levels of particulate organic carbon (POC) in the SML, as TEP attachment to POC may cause TEP to sink out of the SML (Jennings et al. 2017). Both gel particle types did not show consistent changes between day and night. Further analyses will unravel whether or not CSP depletion in the SML is related to a lower production of proteinaceous material by phytoplankton (as indicated by lower chlorophyll-*a* values in the SML), or by higher protein degradation potential in the SML

Iodide dynamics in the SML

The reaction of iodide with ozone at the sea surface is an important removal process for tropospheric ozone (Ganzeveld et al. 2009) and it releases reactive iodine-containing gases to the atmosphere that participate in further atmospheric chemical reactions that ultimately affect air quality and climate (Carpenter et al. 2013; Sherwen et al. 2017). Rates of both ozone loss and air-sea iodine flux are dependent on iodide concentrations at the air-sea interface

(Carpenter et al. 2013). Although progress has been made in predicting iodide concentrations in bulk near-surface seawater (Chance et al. 2014; Sherwen et al. 2019), to date there are very few measurements of iodide concentrations in the SML itself (Chance et al. 2014).

The iodide concentrations observed in this study (168 – 241 nM, average 205 nM, $n = 8$) are within the range of previous measurements made in shelf regions (Truesdale et al. 2003; Truesdale et al. 2001), reflecting a general trend for higher iodide in coastal and estuarine waters at similar latitudes (Chance et al. 2014), but diel variation of iodine speciation in the SML itself has not previously been investigated. A study in the tropical Atlantic found no significant variation in near surface (< 10 m), open ocean iodide concentrations during 24 hours sampling (Chance et al. 2014). During MILAN, Cycle 01 showed no difference between iodide levels in samples collected 1.5 hours after dawn, and samples collected at sunset, consistent with a lack of diel variation. Meanwhile, during Cycle 03, iodide concentrations in both the SML and ULW were higher in samples collected 3 hours after sunset ('night-time') than those collected ~4 hours after dawn ('daytime') (Fig. 13). The causes of these observed differences are not yet clear. Our data show that under certain conditions, iodide concentrations might be enhanced in the SML. However, the extent of this enhancement does not appear to reflect any particular day-night contrast.

Air-sea gas exchange of CO₂

We used a free-drifting buoy to measure temporal change in the partial pressure of CO₂ in a chamber floating on top of the sea surface (Ribas-Ribas et al. 2018a), allowing us to estimate the gas transfer velocity of CO₂ (k ; cm h⁻¹) to high spatial and temporal resolution compared to other techniques. Our k estimates (Fig. 14) are within the range previously estimated in Jade Bay during daytime (Ribas-Ribas et al. 2018a). We observed no significant differences in k between day (mean \pm sd 5.4 \pm 3.5 cm h⁻¹) and night (mean \pm sd 5.1 \pm 5.1 cm h⁻¹). However, with k categorized in terms of low (0-2.5 m s⁻¹), medium (2.5-5 m s⁻¹) and high

(5-10 m s⁻¹) wind speed bins (Fig. 14 B), there was a significant difference between day and night for the low wind bin (Mann-Whitney-U-test, $W = 66$, $p\text{-value} = 0.006$, $n = 18$; Fig. 14 C), but there was no day–night difference for either the moderate or high wind bins.

In the equatorial Pacific, McGillis et al. (2004) reported day-night variation of k , and CO₂ fluxes. They found increases in CO₂ fluxes of up to 40% during nighttime, reflecting coincident strong increases in vertical convective velocity. They concluded that diel heating cycles can sometimes affect k to a larger extent than does wind speed. In Jade Bay during spring, oscillating insolation was not as pronounced as in the equatorial Pacific, and turbulent mixing was probably the dominant process driving gas exchange. Yang et al. (2019) showed diel variability in CO₂ flux associated with diel variability in near surface pCO₂. We also observed diel variability in near surface pCO₂, ranging from 542 μatm at 18:00 to 635 μatm at 07:00. Under these calm conditions, it seems possible to have a vertical gradient in pCO₂ from the measured depth (1.2 m) to the water surface, which would have influenced the gas transfer velocity estimates.

Microsensor studies

To evaluate the respective scales of diffusive and turbulent transport at the sea surface, we used microsensors (Revsbech and Jørgensen (1986) to obtain high-resolution O₂ and pH microprofiles in an aquarium filled with Jade Bay water. Both microsensors had 25-50 μm tip diameters; the pH microsensor was pH sensitive over a tip length of approx. 200 μm .

Figure 15 shows example O₂ and pH microprofiles, and the data show O₂ supersaturation indicative of net photosynthesis, similar to previous experiments conducted with Jade Bay water during summer (Rahlff et al. 2019). Diffusive O₂ transport is evidenced by the linear increase in O₂ concentration from 0 μm to approx. 500 μm depth. Below this diffusive boundary layer, a large change in the O₂ concentration gradient indicates a shift to dominance by turbulent transport, even in an aquarium with no active stirring except that

caused by temperature differences. As the thickness of the diffusive boundary layer decreases with increasing turbulence, this confirms that in most natural systems diffusive transport resistance is within a non-turbulent layer, only fractions of a millimeter deep, and may be even less than in our tank study. The thickness of the diffusive boundary layer under highly turbulent conditions cannot be determined by microsensor profiling, as the sensor itself will create increased turbulence around the sensor tip (Glud et al. 1994). That means that the effective diffusive boundary layer thickness under such conditions has to be determined from rate of bulk gas exchange between water and overlying gas phase.

In the bulk water, pH was alkaline during accompanying CO₂ consumption (Fig. 15), confirming a net photosynthetic history, while surface water pH was more than 0.1 units lower due to CO₂ uptake from the air. The diffusive boundary layer thus exerts a strong resistance to H⁺-diffusion across the uppermost ~500 μm of the sea surface.

Ambient and nascent aerosol particles

The chemical composition of ambient aerosol particles varied strongly during MILAN (Fig. 16 A). Ammonia, nitrate and sulfate were always the dominant inorganic ions. Organic carbon, including both water soluble and water-insoluble components, contributed on average 25% to the identified aerosol mass. Elemental carbon is a tracer of anthropogenic sources, e.g. biomass burning, and was on average five times higher than in “clean” marine samples (Cavalli et al. 2004), indicating a strong anthropogenic signal in Jade Bay. Nevertheless, clear marine source signals were evidenced by elevated sodium and chloride concentrations (e.g. between April 5th and 7th) and/or by significant concentrations of methane sulfonic acid, a decay product of the marine trace gas dimethyl sulfide.

Air mass origin determines the residence time of aerosol particles over the ocean and may eventually influence aerosol composition. We calculated the backwards trajectories for 96 h prior to sampling (details in van Pinxteren et al. (2010)) which additionally showed large

fractions of the aerosol samples collected during MILAN to be of marine origin, especially in the second half of the campaign. Varying day and night contributions to the organic carbon content requires further analysis of the primary and secondary organic carbon constituents.

To improve our understanding of how the organic matter pool in the ULW and the SML influences the flux and composition of nascent sea spray aerosols, and to derive further insights into the qualitative and quantitative transfer of marine organic material into aerosols, we generated nascent sea spray aerosols using a laboratory sea spray aerosol chamber (Salter et al. 2014) in parallel with ambient aerosol collection. The chamber excludes ambient air (e.g. anthropogenic aerosol) and solar radiation so that any chemical evolution of the chamber water is minimized. Alongside measurements of the size and number of particles generated in the chamber, analyses of the chemical composition of the particles were also conducted. Preliminary results revealed significant enrichment of surfactants in the nascent aerosols as well as specific classes of the organic carbon pool such as amino acids.

SUMMARY AND OUTLOOK

MILAN was a truly multidisciplinary, international study involving scientists from the fields of marine (micro)biology, biogeochemistry, marine chemistry, atmospheric chemistry and physics, and physical oceanography. It combined diverse approaches in the field and in the laboratory to study the diel properties of the SML and their effects on the air-sea exchange of climate-relevant gases and aerosols.

MILAN took place in Jade Bay, which is strongly tidally influenced. The large amounts of suspended material in the water may partly account for the strong variability observed, e.g. regarding the biomass and abundance of organisms. Tidal currents generally influence water column properties such as salinity and temperature. During both cycles we followed a free-drifting buoy, and hourly CTD measurements (depth 1.2 – 2 m) confirm that we were able to follow the same water mass (Fig. 6). Nevertheless, salinity and temperature were clearly different between the SML and ULW, suggesting that the SML represents a distinct water layer. SML material and organisms are often recruited from the ULW (Cunliffe et al. 2013), and this transport might be a function of tidal currents velocities. The preliminary analysis of our initial results presented in this publication did not reveal any relationships between current velocities and the enrichment of material and organisms in the SML. Nevertheless, addressing potential tidal effects will be an important focus of our definitive detailed analysis and interpretation. This is currently in progress in all the participating laboratories.

Our initial results point to a radiation-dependence of several SML processes. Some of these support previous observations and conclusions, such as increasing lipid degradation in the SML during the night, which most likely reflects diel changes in the relative importance of phytoplankton production and bacterial degradation. Some of our findings, e.g. the dose-dependent enrichment of the phytoplankton group Cryptophytes in the SML, will help to refine our knowledge of the species-specific occurrence of SML inhabitants. Other results

were seemingly contradictory. For example, while experiments with the solar simulator clearly implied daytime surfactant production, surfactant concentrations in the field were actually highest at night, which has not been reported before. Such contrasts highlight a need to unravel the microbiological and photochemical turnover of surfactants to better understand their dynamics in the natural environment. Another interesting observation of MILAN is that while CDOM enrichment in the SML tends to decrease under highest radiation levels, indicative of well-known photo-bleaching as the main CDOM sink (Nelson and Siegel 2013), CDOM absolute concentrations in the SML do not necessarily follow this pattern. Eventually, the dynamics of organisms and organic material within the SML will feedback into air-sea exchange processes, and our initial data suggest that day and night CO₂ fluxes might differ if wind speed is low ($< 2.5 \text{ m s}^{-1}$).

An important overall conclusion from MILAN is that while prior information on SML function obtained from observational and experimental campaigns carried out during daytime is undoubtedly of great value, future progress in our understanding will require additional information on day-night contrasts. MILAN has shown how the combination of expertise from diverse disciplines as well as the combination of field and laboratory experiments is the most appropriate approach to achieve this. We are convinced that strengthening the links between disciplines is an important step to deepen the first insights presented here, and to further unravel the complexity of air-sea interaction (Engel et al. 2017).

MILAN was performed in the coastal zone, which is of strong importance for biogeochemical cycles (Gattuso et al. 1998) especially considering the strong anthropogenic forcing in coastal habitats (Jickells 1998). Coastal oceans are additionally important areas for air-sea gas-exchange (Upstill-Goddard 2006) and the formation of new aerosol particles (O'Dowd and Hoffmann 2005). Nevertheless, while in coastal regions like Jade Bay high numbers of suspended particles greatly inhibit downward light penetration (Tedetti and

Sempéré 2006), in more oligotrophic systems with lower suspended particle concentrations the contrasting effects of radiation on the biogeochemical properties of the SML and ULW will likely be quite different. Future studies should therefore target a broad range of oceanic regions and seasons (e.g. summer phytoplankton blooms), and we hope that MILAN will stimulate further diel studies of air-sea interface processes. In light of the global importance of matter and energy exchange across the SML, the focus of these should be on improving our understanding of the long- and short-term effects of climate change. We predict that in a future ocean, changes in wind regimes, radiation intensities and precipitation rates will greatly modify SML properties, leading to subsequent feedbacks affecting many aspects of air-sea interaction (Wurl et al. 2017).

ACKNOWLEDGEMENT

The authors would like to acknowledge Dave Carlson, who not only made tremendous scientific contributions to SML research, but who also inspired MILAN through one simple post during our discussion session at SOLAS OSC 2015: NIGHT-TIME!

MILAN would not have been possible without the financial, logistical and personnel support given by CvO University of Oldenburg, ICBM Wilhelmshaven, and Senckenberg Institute Wilhelmshaven. In particular, we thank the following colleagues: Uwe Ebensen, Heike Scheele, Axel Braun, Hanne Marie Banko-Kubis, Tiera-Brandy Robinson, Janina Rahlff, Michaela Christine Haack, Katharina Melkonian-Ezekian, Sibet Riexinger, Helmo Nicolai, Jonathan Barnes, Ingrid Kröncke, and the captains and crews of RVs Senckenberg, Otzum and Zephyr.

MILAN received substantial support from the European Research Council project PASSME (grant GA336408) awarded to O. Wurl, and the following funding sources were also crucial: European Union's Horizon 2020 research and innovation program under the Marie Skłodowska-Curie grant agreement 702747 – *POSEIDOMM* (to L. Galgani); European Union Seventh Framework Programme (FP7 2007-2013) Marie Curie FP7-PEOPLE-2011-COFUND (GA no 291823) through NEWFELPRO project (Contract 47) (to S. Frka); Croatian Science Foundation under the project IP-11-2013-8607 (to B. Gašparović); UCR-B8068 grant under project "Energy, water vapour and CO₂ transport: analysis of turbulent fluxes" and UCR-IsoNet (to A.M. Durán Quesada); School of Marine Science and Technology, Newcastle University (to P. Rickard, R. Upstill-Goddard, G. Uher); Lyell Centre, Heriot-Watt University (to R. Pereira); Leibniz Association project MarParCloud, SAW-2016-TROPOS-2 (to M. van Pinxteren, N. Triesch, C. Stolle); Swedish Vetenskapsrådet under the project 2016-05100 (to M. Salter); UK Natural Environment Research Council (NERC) grant NE/N009983/1 (to L. Carpenter, R. Chance) and NERC PhD studentship via the SPHERES DTP (to A. Saint); COD project (VWZN3175) funded by

571 Lower Saxony Ministry of Science and Culture (to M. Striebel); the Poul Due Jensen
572 Foundation (to N.P. Revsbech).
573

REFERENCES

- Alpert, P. A., and Coauthors, 2017: Fatty acid surfactant photochemistry results in new particle formation. *Sci. Rep.-UK*, **7**, 12693.
- Asher, W., 2009: The effects of experimental uncertainty in parameterizing air-sea gas exchange using tracer experiment data. *Atmos. Chem. Phys.*, **9**, 131-139.
- Azam, F., and F. Malfatti, 2007: Microbial structuring of marine ecosystems. *Nat. Rev. Microbiol.*, **5**, 782.
- Bigg, E. K., and C. Leck, 2008: The composition of fragments of bubbles bursting at the ocean surface. *J. Geophys. Res.: Atmos.*, **113**, D11209, doi: 10.1029/2007JD009078.
- Broecker, W. S., and T.-H. Peng, 1974: Gas exchange rates between air and sea. *Tellus*, **26**, 21-35.
- Bunker, A. F., 1976: Computations of surface energy flux and annual air-sea interaction cycles of the North Atlantic Ocean. *Mon. Weather Rev.*, **104**, 1122-1140.
- Calleja, M. L., C. M. Duarte, N. Navarro, and S. Agustí, 2005: Control of air-sea CO₂ disequilibria in the subtropical NE Atlantic by planktonic metabolism under the ocean skin. *Geophys. Res. Lett.*, **32**, L08606, doi: 10.1029/2004GL022120.
- Carlucci, A. F., D. B. Craven, K. J. Robertson, and P. M. Williams, 1986: Surface-film microbial populations: diel amino acid metabolism, carbon utilization, and growth rates. *Mar. Biol.*, **92**, 289-297.
- Carpenter, L. J., and P. D. Nightingale, 2015: Chemistry and Release of Gases from the Surface Ocean. *Chem. Sci.*, **115**, 4015-4034.
- Carpenter, L. J., and Coauthors, 2013: Atmospheric iodine levels influenced by sea surface emissions of inorganic iodine. *Nat. Geosci.*, **6**, 108-111.
- Cavalli, F., and Coauthors, 2004: Advances in characterization of size-resolved organic matter in marine aerosol over the North Atlantic. *J. Geophys. Res.: Atmos.*, **109**, D24215, doi: 10.1029/2004JD005137.
- Chance, R., A. R. Baker, L. Carpenter, and T. D. Jickells, 2014: The distribution of iodide at the sea surface. *Environ. Sci.-Proc. Imp*, **16**, 1841-1859.
- Chin, W.-C., M. V. Orellana, and P. Verdugo, 1998: Spontaneous assembly of marine dissolved organic matter into polymer gels. *Nature*, **391**, 568-572.
- Christodoulou, S., J.-C. Marty, J.-C. Miquel, J. K. Volkman, and J.-F. Rontani, 2009: Use of lipids and their degradation products as biomarkers for carbon cycling in the northwestern Mediterranean Sea. *Mar. Chem.*, **113**, 25-40.
- Ciuraru, R., L. Fine, M. van Pinxteren, B. D'Anna, H. Herrmann, and C. George, 2015: Photosensitized production of functionalized and unsaturated organic compounds at the air-sea interface. *Sci. Rep.-UK*, **5**, 12741.
- Colijn, F., and G. C. Cadée, 2003: Is phytoplankton growth in the Wadden Sea light or nitrogen limited? *J. Sea Res.*, **49**, 83-93.
- Colijn, F., K.-J. Hesse, N. Ladwig, and U. Tillmann, 2002: Effects of the large-scale uncontrolled fertilisation process along the continental coastal North Sea. *Sustainable Increase of Marine Harvesting: Fundamental Mechanisms and New Concepts*, O. Vadstein, and Y. Olsen, Eds., Kluwer Academic Publisher, 133-148.
- Cunliffe, M., and J. C. Murrell, 2009: Eukarya 18S rRNA gene diversity in the sea surface microlayer: implications for the structure of the neustonic microbial loop. *ISME J*, **4**, 455-458.
- Cunliffe, M., and Coauthors, 2013: Sea surface microlayers: A unified physicochemical and biological perspective of the air-ocean interface. *Prog. Oceanogr.*, **109**, 104-116.
- Curry, J. A., and E. E. Ebert, 1992: Annual cycle of radiation fluxes over the Arctic Ocean: Sensitivity to cloud optical properties. *J. Clim.*, **5**, 1267-1280.
- Engel, A., and Coauthors, 2017: The Ocean's Vital Skin: Toward an Integrated Understanding of the Sea Surface Microlayer. *Front. Mar. Sci.*, **4**, 165, doi: 10.3389/fmars.2017.00165.
- Falkowska, L., 2001: 12-hour cycle of matter transformation in the sea surface microlayer in the offshore waters of the Gdańsk Basin (Baltic Sea) during spring. *Oceanologia*, **43**.

Farmer, D., C. McNeil, and B. Johnson, 1993: Evidence for the importance of bubbles in increasing air–sea gas flux. *Nature*, **361**, 620.

Frew, N. M., R. K. Nelson, and C. G. Johnson, 2006: Sea slicks: variability in chemical composition and surface elasticity. *Marine Surface Films*, M. Gade, H. Hühnerfuss, and G. Korenowski, Eds., Springer, 45–56.

Frew, N. M., J. C. Goldman, M. R. Dennett, and A. S. Johnson, 1990: Impact of phytoplankton-generated surfactants on air-sea gas exchange. *J. Geophys. Res.: Oceans*, **95**, 3337–3352.

Galgani, L., J. Piontek, and A. Engel, 2016: Biopolymers form a gelatinous microlayer at the air-sea interface when Arctic sea ice melts. *Sci. Rep.-UK*, **6**, 29465.

Ganzeveld, L., D. Helmig, C. W. Fairall, J. Hare, and A. Pozzer, 2009: Atmosphere-ocean ozone exchange: A global modeling study of biogeochemical, atmospheric, and waterside turbulence dependencies. *Global Biogeochem. Cy.*, **23**, GB4021, doi:4010.1029/2008GB003301.

Gašparović, B., B. Čosović, and V. Vojvodić, 1998: Contribution of organic acids to the pool of surface active substances in model and marine samples using o-nitrophenol as an electrochemical probe. *Org. Geochem.*, **29**, 1025–1032.

Gašparović, B., and Coauthors, 2014: Factors influencing particulate lipid production in the East Atlantic Ocean. *Deep-Sea Res. Pt. I*, **89**, 56–67.

Gattuso, J.-P., M. Frankignoulle, and R. Wollast, 1998: Carbon and carbonate metabolism in coastal aquatic ecosystems. *Annu. Rev. Ecol. Syst.*, **29**, 405–434.

Gladyshev, M., 2002: *Biophysics of the surface microlayer of aquatic ecosystems*. IWA Publishing.

Glud, R.N., J.K. Gundersen, N.P. Revsbech & B.B. Jørgensen, 1994: Effects on the benthic diffusive boundary layer imposed by microelectrodes. *Limnol. Oceanogr.*, **39**: 462–467.

Götschenberg, A., and A. Kahlfeld, 2008: The Jade. *Die Küste*, **74**, 263–274.

Guitart, C., N. García-Flor, J. M. Bayona, and J. Albaigés, 2007: Occurrence and fate of polycyclic aromatic hydrocarbons in the coastal surface microlayer. *Mar. Pollut. Bull.*, **54**, 186–194.

Häder, D.-P., and Coauthors, 2015: Effects of UV radiation on aquatic ecosystems and interactions with other environmental factors. *Photochem. Photobio. S.*, **14**, 108–126.

Hardy, J. T., 1982: The sea surface microlayer: Biology, chemistry and anthropogenic enrichment. *Prog. Oceanogr.*, **11**, 307–328.

Helms, J. R., A. Stubbins, J. D. Ritchie, E. C. Minor, D. J. Kieber, and K. Mopper, 2008: Absorption spectral slopes and slope ratios as indicators of molecular weight, source, and photobleaching of chromophoric dissolved organic matter. *Limnol. Oceanogr.*, **53**, 955–969.

Holdway, P., and L. Maddock, 1983: A comparative survey of neuston: geographical and temporal distribution patterns. *Mar. Biol.*, **76**, 263–270.

Jähne, B., 2009: Air–sea gas exchange. *Elements of Physical Oceanography: A Derivative of the Encyclopedia of Ocean Sciences*, 160–169.

Jennings, M. K., U. Passow, A. S. Wozniak, and D. A. Hansell, 2017: Distribution of transparent exopolymer particles (TEP) across an organic carbon gradient in the western North Atlantic Ocean. *Mar. Chem.*, **190**, 1–12.

Jessup, A., C. Zappa, V. Hesany, M. Loewen, and M. Skafel, 1995: Dependence of the skin layer recovery rate on heat flux and turbulence. *Air-Water Gas Transfer*, B. Jähne, and E. C. Monahan, Eds., AEON Verlag & Studio, 601–610.

Jessup, A., W. Asher, M. Atmane, K. Phadnis, C. J. Zappa, and M. Loewen, 2009: Evidence for complete and partial surface renewal at an air-water interface. *Geophys. Res. Lett.*, **36**.

Jickells, T. D., 1998: Nutrient Biogeochemistry of the Coastal Zone. *Science*, **281**, 217–222.

Joux, F., H. Agogué, I. Obernosterer, C. Dupuy, T. Reinthaler, G. J. Herndl, and P. Lebaron, 2006: Microbial community structure in the sea surface microlayer at two contrasting coastal sites in the northwestern Mediterranean Sea. *Aquat. Microb. Ecol.*, **42**, 91–104.

Katsaros, K. B., 1980: The aqueous thermal boundary layer. *Boundary Layer Meteorol.*, **18**, 107–127.

Kattner, G., and U. Brockmann, 1978: Fatty-acid composition of dissolved and particulate matter in surface films. *Mar. Chem.*, **6**, 233–241.

676 Kujawinski, E. B., J. W. Farrington, and J. W. Moffett, 2002: Evidence for grazing-mediated production
677 of dissolved surface-active material by marine protists. *Mar. Chem.*, **77**, 133-142.

678 Kuznetsova, M., C. Lee, J. Aller, and N. Frew, 2004: Enrichment of amino acids in the sea surface
679 microlayer at coastal and open ocean sites in the North Atlantic Ocean. *Limnol. Oceanogr.*, **49**, 1605-
680 1619.

681 Latham, J., and Coauthors, 2008: Global temperature stabilization via controlled albedo
682 enhancement of low-level maritime clouds. *Philos. Trans. R. Soc. Lond., Ser. A*, **366**, 3969-3987.

683 Lechtenfeld, O. J., B. P. Koch, B. Gašparović, S. Frka, M. Witt, and G. Kattner, 2013: The influence of
684 salinity on the molecular and optical properties of surface microlayers in a karstic estuary. *Mar.*
685 *Chem.*, **150**, 25-38.

686 Maki, J. S., and R. P. Herwig, 1991: A diel study of the neuston and plankton bacteria in an Antarctic
687 pond. *Antarct. Sci.*, **3**, 47-51.

688 McGillis, W. R., and Coauthors, 2004: Air-sea CO₂ exchange in the equatorial Pacific. *J. Geophys. Res.: Oceans*, **109**, C08S02.

690 Memery, L., and L. Merlivat, 1985: Modelling of gas flux through bubbles at the air-water interface. *Tellus*, **37B**, 272-285.

692 Mobasher, M. R., 2006: Reformation time for the thermal skin layer of the ocean. *Int. J. Remote Sens.*, **27**, 5285-5299.

694 Mopper, K., D. J. Kieber, and A. Stubbins, 2015: Chapter 8 - Marine Photochemistry of Organic
695 Matter: Processes and Impacts. *Biogeochemistry of Marine Dissolved Organic Matter (Second Edition)*, D. A. Hansell, and C. A. Carlson, Eds., Academic Press, 389-450.

697 Murray, B., D. O'sullivan, J. Atkinson, and M. Webb, 2012: Ice nucleation by particles immersed in
698 supercooled cloud droplets. *Chem. Soc. Rev.*, **41**, 6519-6554.

699 Mustafa, N. I. H., M. Ribas-Ribas, H. M. Banko-Kubis, and O. Wurl, in preparation: *In situ* CO₂ transfer
700 velocity reduction by natural surfactants in the sea surface microlayer.

701 Nelson, N. B., and D. A. Siegel, 2013: The global distribution and dynamics of chromophoric dissolved
702 organic matter. *Annu. Rev. Marine Sci.*, **5**, 447-476.

703 O'Dowd, C. D., and T. Hoffmann, 2005: Coastal New Particle Formation: A Review of the Current
704 State-Of-The-Art. *Environ. Chem.*, **2**, 245-255.

705 Ocampo-Torres, F., M. Donelan, N. Merzi, and F. Jia, 1994: Laboratory measurements of mass
706 transfer of carbon dioxide and water vapour for smooth and rough flow conditions. *Tellus*, **46B**, 16-
707 32.

708 Otto, L., J. Zimmerman, G. Furnes, M. Mork, R. Saetre, and G. Becker, 1990: Review of the physical
709 oceanography of the North Sea. *Neth J. Sea Res.*, **26**, 161-238.

710 Passow, U., 2002: Production of transparent exopolymer particles (TEP) by phyto-and
711 bacterioplankton. *Mar. Ecol. Prog. Ser.*, **236**, 1-12.

712 Pereira, R., K. Schneider-Zapp, and R. C. Upstill-Goddard, 2016: Surfactant control of gas transfer
713 velocity along an offshore coastal transect: results from a laboratory gas exchange tank. *Biogeosciences*, **13(13)**, 3981-3989.

715 Pereira, R., I. Ashton, B. Sabbaghzadeh, J. D. Shutler, and R. C. Upstill-Goddard, 2018: Reduced air-
716 sea CO₂ exchange in the Atlantic Ocean due to biological surfactants. *Nat. Geosci.*, **11**, 492-496.

717 Quinn, P. K., D. B. Collins, V. H. Grassian, K. A. Prather, and T. S. Bates, 2015: Chemistry and Related
718 Properties of Freshly Emitted Sea Spray Aerosol. *Chem. Sci.*, **115**, 4383-4399.

719 Rahlff, J., C. Stolle, H.-A. Giebel, M. Ribas-Ribas, L. R. Damgaard, and O. Wurl, 2019: Oxygen profiles
720 across the sea-surface microlayer - effects of diffusion and biological activity. *Front. Mar. Sci.*, **6**: **11**.

721 Rahlff, J., C. Stolle, H.-A. Giebel, T. Brinkhoff, M. Ribas-Ribas, D. Hodapp, and O. Wurl, 2017: High
722 wind speeds prevent formation of a distinct bacterioneuston community in the sea-surface
723 microlayer. *FEMS Microbiol. Ecol.*, **93**, fix041.

724 Revsbech, N. P., and B. B. Jørgensen, 1986: Microelectrodes: their use in microbial ecology. *Adv. Microb. Ecol.*, K. C. Marshall, Ed., Springer, 293-352.

726 Ribas-Ribas, M., L. F. Kilcher, and O. Wurl, 2018a: *Sniffle*: a step forward to measure *in situ* CO₂ fluxes
 727 with the floating chamber technique. *Elem Sci Anth*, **6** (1): **14**,
 728 <https://doi.org/10.1525/elementa.1275>.
 729 Ribas-Ribas, M., F. Helleis, J. Rahlff, and O. Wurl, 2018b: Air-sea CO₂-exchange in a large annular
 730 wind-wave tank and the effects of surfactants. *Front. Mar. Sci.*, 10.3389/fmars.2018.00457.
 731 Ribas-Ribas, M., N. I. H. Mustaffa, J. Rahlff, C. Stolle, and O. Wurl, 2017: Sea Surface Scanner (S³): A
 732 catamaran for high-resolution measurements of biogeochemical properties of the sea surface
 733 microlayer. *J Atmos Ocean Tech*, **34**, 1433-1448.
 734 Robinson, T. B., E. Bahlmann, K. Jürgens, O. Wurl, and C. Stolle, 2019: Rising bubbles enhance the
 735 gelatinous nature of the air-sea interface. *Limnol. Oceanogr.*, doi: **10.1002/lno.11188**.
 736 Sabbaghzadeh, B., R. C. Upstill-Goddard, R. Beale, R. Pereira, and P. D. Nightingale, 2017: The Atlantic
 737 Ocean surface microlayer from 50°N to 50°S is ubiquitously enriched in surfactants at wind speeds up
 738 to 13 m s⁻¹. *Geophys. Res. Lett.*, **44**, 2852-2858.
 739 Salter, M., and Coauthors, 2011: Impact of an artificial surfactant release on air-sea gas fluxes during
 740 Deep Ocean Gas Exchange Experiment II. *J. Geophys. Res.: Oceans*, **116**, C11016,
 741 doi:10.1029/12011JC007023.
 742 Salter, M. E., E. D. Nilsson, A. Butcher, and M. Bilde, 2014: On the seawater temperature dependence
 743 of the sea spray aerosol generated by a continuous plunging jet. *J. Geophys. Res.: Atmos.*, **119**, 9052-
 744 9072.
 745 Santos, A. L., C. Mendes, N. C. M. Gomes, I. Henriques, A. Correia, A. Almeida, and Â. Cunha, 2009:
 746 Short-term variability of abundance, diversity and activity of estuarine bacterioneuston and
 747 bacterioplankton. *J. Plankton Res.*, **31**, 1545-1555.
 748 Satpute, S. K., I. M. Banat, P. K. Dhakephalkar, A. G. Banpurkar, and B. A. Chopade, 2010:
 749 Biosurfactants, bioemulsifiers and exopolysaccharides from marine microorganisms. *Biotechnol.*
 750 *Adv.*, **28**, 436-450.
 751 Saunders, P. M., 1967: The temperature at the ocean-air interface. *J. Atm. Sci.*, **24**, 269-273.
 752 Schlitzer, R., 2017, Ocean Data View, <https://odv.awi.de/>.
 753 Schlüssel, P., A. V. Soloviev, and W. J. Emery, 1997: Cool and freshwater skin of the ocean during
 754 rainfall. *Boundary Layer Meteorol.*, **82**, 439-474.
 755 Schulz, K. G., and Coauthors, 2013: Temporal biomass dynamics of an Arctic plankton bloom in
 756 response to increasing levels of atmospheric carbon dioxide. *Biogeosciences*, **10**, 161-180.
 757 Sherwen, T., R. J. Chance, L. Tinel, D. Ellis, M. J. Evans, and L. J. Carpenter, 2019: A machine learning
 758 based global sea-surface iodide distribution. *Earth Syst. Sci. Data Discuss.*, **2019**, 1-40.
 759 Sherwen, T., and Coauthors, 2017: Effects of halogens on European air-quality. *Faraday Discuss*, **200**,
 760 75-100.
 761 Sieburth, J. M., and J. T. Conover, 1965: Slicks associated with *Trichodesmium* Blooms in the Sargasso
 762 Sea. *Nature*, **205**, 830-831.
 763 Sieburth, J. M., and Coauthors, 1976: Dissolved organic matter and heterotrophic microneuston in
 764 the surface microlayers of the North Atlantic. *Science*, **194**, 1415-1418.
 765 Smyth, T., 2011: Penetration of UV irradiance into the global ocean. *J. Geophys. Res.: Oceans*, **116**,
 766 C11020, doi:10.1029/12011JC007183.
 767 Stolle, C., M. Labrenz, C. Meeske, and K. Jürgens, 2011: The bacterioneuston community structure of
 768 the southern Baltic Sea and its dependence on meteorological conditions. *Appl. Environ. Microbiol.*,
 769 **77**, 3726-3733.
 770 Tanimoto, Y., and S.-P. Xie, 2002: Inter-hemispheric decadal variations in SST, surface wind, heat flux
 771 and cloud cover over the Atlantic Ocean. *J. Meteor. Soc. Japan*, **80**, 1199-1219.
 772 Tedetti, M., and R. Sempéré, 2006: Penetration of ultraviolet radiation in the marine environment. A
 773 review. *Photochem. Photobiol.*, **82**, 389-397.
 774 Tilstone, G. H., R. L. Airs, V. Martinez-Vicente, C. Widdicombe, and C. Llewellyn, 2010: High
 775 concentrations of mycosporine-like amino acids and colored dissolved organic matter in the sea
 776 surface microlayer off the Iberian Peninsula. *Limnol. Oceanogr.*, **55**, 1835-1850.

- Truesdale, V., D. S. Danielssen, and T. J. Waite, 2003: Summer and winter distributions of dissolved iodine in the Skagerrak. *Estuar. Coast. Shelf S.*, **57**, 701-713.
- Truesdale, V. W., G. Nausch, and A. Baker, 2001: The distribution of iodine in the Baltic Sea during summer. *Mar. Chem.*, **74**, 87-98.
- Upstill-Goddard, R. C., 2006: Air–sea gas exchange in the coastal zone. *Estuar. Coast. Shelf S.*, **70**, 388-404.
- van de Poll, W. H., A.-C. Alderkamp, P. J. Janknegt, J. Roggeveld, and A. G. J. Buma, 2006: Photoacclimation modulates excessive photosynthetically active and ultraviolet radiation effects in a temperate and an Antarctic marine diatom. *Limnol. Oceanogr.*, **51**, 1239-1248.
- Van Mooy, B. A., G. Rocap, H. F. Fredricks, C. T. Evans, and A. H. Devol, 2006: Sulfolipids dramatically decrease phosphorus demand by picocyanobacteria in oligotrophic marine environments. *Proc. Natl. Acad. Sci.*, **103**, 8607-8612.
- van Pinxteren, D., E. Brüggemann, T. Gnauk, K. Müller, C. Thiel, and H. Herrmann, 2010: A GIS based approach to back trajectory analysis for the source apportionment of aerosol constituents and its first application. *J. Atmos. Chem.*, **67**, 1-28.
- Wandschneider, K., 1979: Vertical distribution of phytoplankton during investigations of a natural surface film. *Mar. Biol.*, **52**, 105-111.
- Wanninkhof, R., 2014: Relationship between wind speed and gas exchange over the ocean revisited. *Limnol. Oceanogr. Methods*, **12**, 351-362.
- Wanninkhof, R., W. E. Asher, D. T. Ho, C. Sweeney, and W. R. McGillis, 2009: Advances in quantifying air–sea gas exchange and environmental forcing. *Annu. Rev. Marine Sci.*, **1**, 213-244.
- Watanabe, M., Y. Kamae, H. Shiogama, A. M. DeAngelis, and K. Suzuki, 2018: Low clouds link equilibrium climate sensitivity to hydrological sensitivity. *Nat Clim Change*, **8**, 901–906.
- Wilson, T. W., and Coauthors, 2015: A marine biogenic source of atmospheric ice-nucleating particles. *Nature*, **525**, 234-238.
- Wurl, O., and M. Holmes, 2008: The gelatinous nature of the sea-surface microlayer. *Mar. Chem.*, **110**, 89-97.
- Wurl, O., W. Ekau, W. M. Landing, and C. J. Zappa, 2017: Sea surface microlayer in a changing ocean—A perspective. *Elem Sci Anth*, **5**, 31, doi: <https://doi.org/10.1525/elementa.1228>.
- Wurl, O., E. Wurl, L. Miller, K. Johnson, and S. Vagle, 2011: Formation and global distribution of sea–surface microlayers. *Biogeosciences*, **8**, 121-135.
- Wurl, O., C. Stolle, C. Van Thuoc, P. The Thu, and X. Mari, 2016: Biofilm-like properties of the sea surface and predicted effects on air-sea CO₂ exchange. *Prog. Oceanogr.*, **144**, 15-24.
- Wurl, O., and Coauthors, 2018: Warming and Inhibition of Salinization at the Ocean's Surface by Cyanobacteria. *Geophys. Res. Lett.*, **45**, 45, <https://doi.org/10.1029/2018GL077946>.
- Yang, M., and Coauthors, 2019: Insights from year-long measurements of air–water CH₄ and CO₂ exchange in a coastal environment. *Biogeosciences*, **16**, 961-978.
- Zhou, J., K. Mopper, and U. Passow, 1998: The role of surface-active carbohydrates in the formation of transparent exopolymer particles by bubble adsorption of seawater. *Limnol. Oceanogr.*, **43**, 1860-1871.
- Žutić, V., B. Čosović, E. Marčenko, N. Bihari, and F. Kršinić, 1981: Surfactant production by marine phytoplankton. *Mar. Chem.*, **10**, 505-520.

819

MILAN OBJECTIVES (BOX 1)

Most of our knowledge about SML properties and its functional roles derives from observations made during daytime, which is largely a consequence of logistical constraints in the field. Thus, the motivation behind MILAN was the urgent need to study the extent of diel variability in the coupling between meteorological forcing, SML physico-chemical and biological properties, and the air-sea exchange of e.g. CO₂ and aerosol particles.

The several field platforms and laboratory experiments comprising MILAN (Fig. 1) together addressed the following overarching research questions:

1. Does solar radiation cause diel changes in microbial community composition and food web functioning in the SML that are distinct from those in the underlying bulk water?
2. Does the concentration and composition of organic material and other biogeochemically active chemical components (e.g. iodide) in the SML reflect diel patterns of biological and/or photochemical turnover?
3. Is the diel variability of organic material, e.g. surfactants, and biological productivity in the SML sufficient to influence CO₂ fluxes across the SML?
4. Does the composition of organic matter in sea spray aerosol depend on diel transformation of organic material in the SML?

FIGURE CAPTION LIST

Figure 1: Overview of sampling platforms used and laboratory experiments conducted during the MILAN campaign. Sampling platforms in the field included the radio-controlled catamaran S^3 (A, B) to sample the sea surface microlayer (SML) and underlying water (ULW), a free-drifting buoy (C, D) to measure air-sea exchange of CO_2 , and three R/Vs (E, F) to sample the water column. Land-based instruments were deployed to record meteorological data at the ICBM building (G,) and to sample ambient aerosols (H). Laboratory experiments involved a gas-exchange tank (I), a solar simulator (J), a sea spray simulation chamber (K) and microsensor studies (L).

Figure 2: Study area in the coastal North Sea (A) using Ocean Data View (Schlitzer 2017, Ocean Data View, <https://odv.awi.de/>). A detailed view of the drifting courses following tidal currents for the two diel cycles Cycle 01 (B) and Cycle 03 (C) is shown. Asterisk shows location of the land-based weather station and the aerosol sampler.

Figure 3: Mean Sea Level pressure (hPa) in blue to green contours and 10 m wind (black vector arrows) for Cycles 01 (A) and 03 (B). Low level cloud fraction for Cycles 01 (C) and 03 (D). All data was generated from average ERA-Interim (Dee et al. 2011). The location of Jade Bay is shown by the blue box.

Figure 4: Solar Radiation (black circles) and photosynthetically active radiation (PAR; 410-655 nm, blue circles) for Cycles 01 (A) and 03 (B). Air temperature (black line), and water temperature in the sea surface microlayer (SML, blue line), underlying water (ULW, red line) and surface layer CTD (grey circles) for Cycles 01 (C) and 03 (D). Wind speed for Cycles 01 (E) and 03 (F) measured at the land-based weather station.

Figure 5: Current velocities measured during Cycle 01 (A) and Cycle 03 (B). Data were recorded in 3.6 to 4.6 m water depth (Cycle 01) and 1.7 to 2.7 m water depth (Cycle 03).

Figure 6: Temperature-salinity (T-S) diagram of (A) the sea surface microlayer (SML) and (B) the underlying water (ULW) and at the surface layer CTD (1.3 to 2 m depth) during Cycle

03. Day and Night measurements for SML and ULW are shown in red and blue color, respectively.

Figure 7: Biological parameters including Chlorophyll-a (A, B), the relative abundance of the phytoplankton group Chryptophytes (C,D), and bacterial abundance (E, F) during Cycles 01 (green) and 03 (blue). Results are shown as enrichment factor (relative concentration of a parameter x in the sea surface microlayer (SML) vs underlying water (ULW), i.e. $EF = SML[x] / ULW [x]$). EFs are plotted over time (A, C, E) and against solar radiation (B, D, F). Night samples taken at very low wind speed ($\leq 1 \text{ m s}^{-1}$) are marked (yellow asterisk).

Figure 8: (A) Dissolved organic matter (DOM) composition of the different fractions identified in samples from the sea surface microlayer (SML) and underlying water (ULW) from Cycle 03. Additionally, dissolved organic carbon (DOC) concentration is shown as black diamonds. Error bars show standard deviation ($n = 9$) (B) The enrichment factor of the DOM fraction ‘biopolymers’ (i.e. $EF = SML[\text{biopolymers}] / ULW[\text{biopolymers}]$) is plotted against Chlorophyll-a.

Figure 9: (A) Absorption coefficient (m^{-1}) of CDOM at 355 nm wavelength (λ) in sea surface microlayer (SML) samples during Cycle 01 (green) and Cycle 03 (blue). (B) Enrichment factor of $a_{(355 \text{ nm})}$ (i.e. $EF = SML[a_{(355 \text{ nm})}] / \text{underlying water (ULW)}[a_{(355 \text{ nm})}]$) against solar radiation. Night samples taken at very low wind speed ($\leq 1 \text{ m s}^{-1}$) are marked (yellow asterisk). (C) High resolution (0.1 Hz) of in-situ fDOM in the SML and ULW, and (D) histogram of enrichment factor (EF) of fDOM in the SML during day and night at different wind regimes.

Figure 10: (A) Variability of surfactant concentration in the sea surface microlayer (SML, triangles) and underlying water (ULW, squares), and enrichment factors (EF, circles) during Cycle 03. (B) Changes in SML surfactant concentration during irradiance (red diamonds) compared to dark (black diamonds) and temperature controls (open diamonds) in the solar simulator.

Figure 11: Concentrations of particulate lipids (A, B) and their degradation index (C, D) of some sea surface microlayer (SML) and underlying water (ULW) samples taken during Cycle 01 (green) and 03 (blue). Error bars show standard deviation of duplicate measurements.

Figure 12: Box-whisker plot of the abundance of (A) Coomassie Stainable Particles (CSP) and (B) Transparent Exopolymer Particles (TEP) of sea surface microlayer (SML) and underlying water (ULW) samples taken during day and night. Combined data of Cycle 01 and 03 is shown. The boxes show the median (line) and the range of data from 25th and 75th percentiles ($n = 8-10$).

Figure 13: Iodide concentrations in filtered underlying water (ULW) and sea surface microlayer (SML) samples taken during Cycle 01 (green) and Cycle 03 (blue). Error bars show range (where $n=2$) or standard deviation (where $n>2$) of replicate measurements.

Figure 14: Box-whisker plots of the gas transfer velocities k for (A) day and night; (B) different wind speed bins; and (C) day and night for the low wind speed bin ($< 2.5 \text{ m s}^{-1}$). The boxes show the median (line) and the range of data from 25th and 75th percentiles; whiskers represent the 5th and 95th percentiles.

Figure 15: Example gradients of oxygen (red) and pH (blue) across the air-sea interface measured with microsensors in an aquarium filled with Jade Bay water.

Figure 16: The respective contribution of different chemical species to the composition of the PM_{10} aerosol particles including the main inorganic ions as well as organic carbon differentiated between water soluble organic carbon (WSOC) and water-insoluble organic carbon (WISOC). The residence time of the air masses over water and ice ($RT_{\text{water and ice}}$) is also shown.

913 **Table 1:** Summary of field and laboratory experiments performed during MILAN (* Test Experiment; # Experiment aborted due to strong wind)

Field	Experiment Start /End	Location	High tide	Low tide	Sunrise	Sunset
Experiments	Date / Time (UTC)		Time (UTC)	Time (UTC)	Time (UTC)	Time (UTC)
Cycle 0*	Start: April 3 rd 2017 / 09:30 End: April 3 rd 2017 / 13:30	Jade Bay	06:08, 18:26	-, 12:09	06:54	20:07
Cycle 1	Start: April 4 th 2017 / 07:15 End: April 5 th 2017 / 09:30	Jade Bay	06:58, 19:20 08:04, 20:35	00:29, 12:53 01:26, 13:59	06:51 06:49	20:08 20:10
Cycle 2 [#]	Start: April 6 th 2017 / 08:30 End: April 6 th 2017 / 15:00	Jade Bay	09:30, 22:05	02:47, 15:28	06:46	20:12
Cycle 3	Start: April 8 th 2017 / 07:30 End: April 9 th 2017 / 09:00	Jade Bay	-, 12:12 00:28, 13:02	05:43, 18:10 06:39, 18:58	06:42 06:39	20:16 20:18
Cycle 4	Start: April 10 th 2017 / 10:00 End: April 11 th 2017 / 10:00	Wilhelmshaven Harbour	01:13, 13:42 01:54, 14:21	07:21, 19:39 08:02, 20:21	06:37 06:35	20:19 20:21

914

915

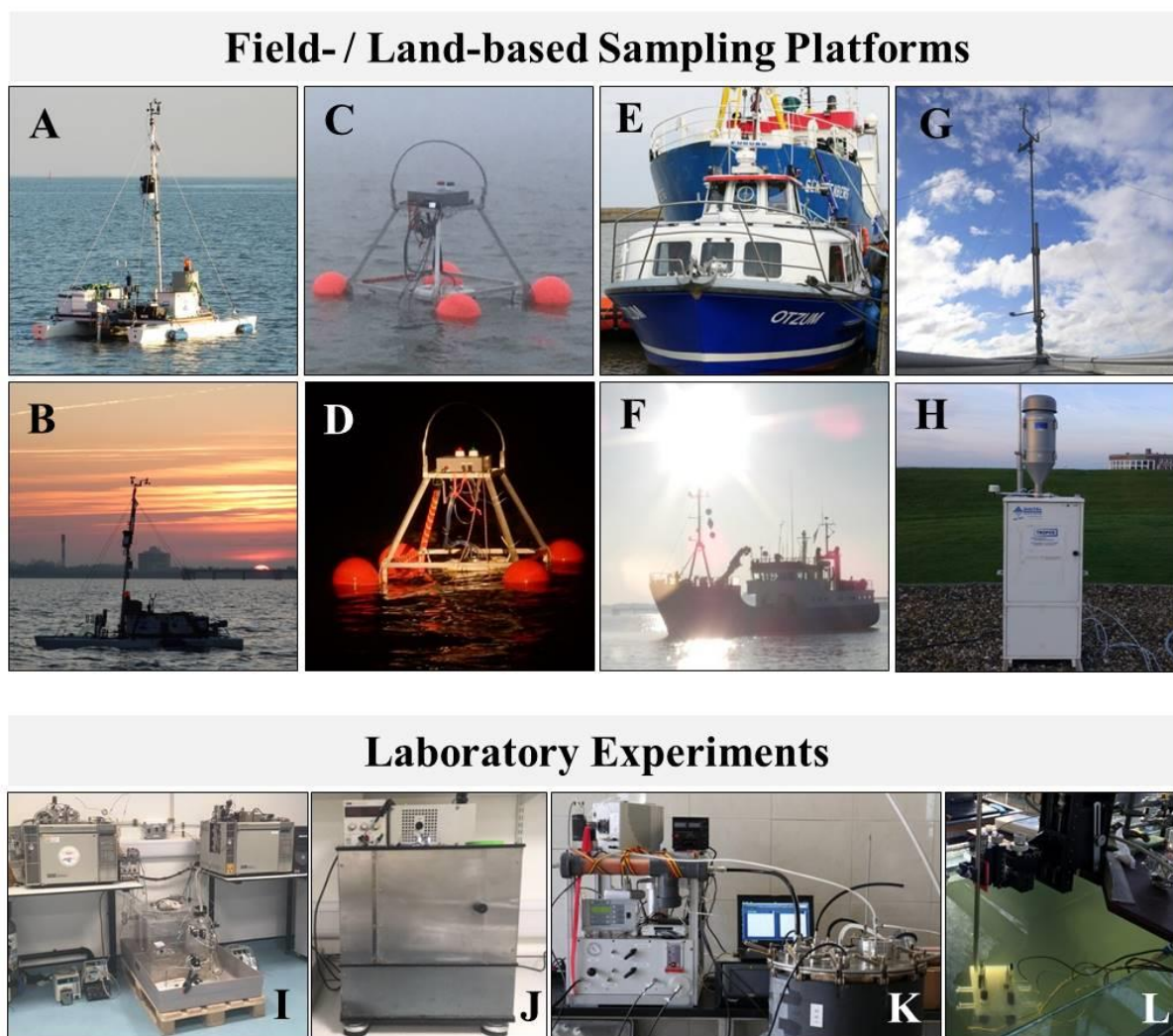


Figure 1: Overview of sampling platforms used and laboratory experiments conducted during the MILAN campaign. Sampling platforms in the field included the radio-controlled catamaran S^3 (A, B) to sample the sea surface microlayer (SML) and underlying water (ULW), a free-drifting buoy (C, D) to measure air-sea exchange of CO_2 , and three R/Vs (E, F) to sample the water column. Land-based instruments were deployed to record meteorological data at the ICBM building (G,) and to sample ambient aerosols (H). Laboratory experiments involved a gas-exchange tank (I), a solar simulator (J), a sea spray simulation chamber (K) and microsensor studies (L).

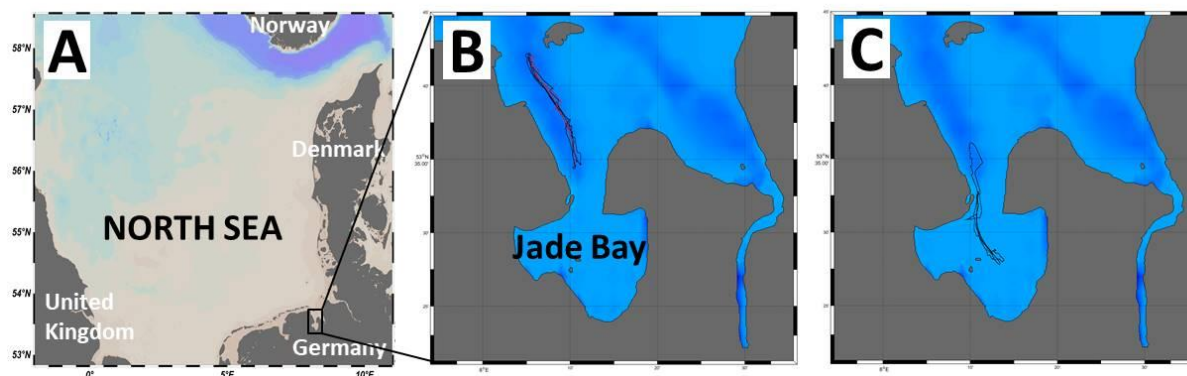


Figure 2: Study area in the coastal North Sea (A) using Ocean Data View (Schlitzer 2017, Ocean Data View, <https://odv.awi.de/>). A detailed view of the drifting courses following tidal currents for the two diel cycles Cycle 01 (B) and Cycle 03 (C) is shown. Asterisk shows location of the land-based weather station and the aerosol sampler.

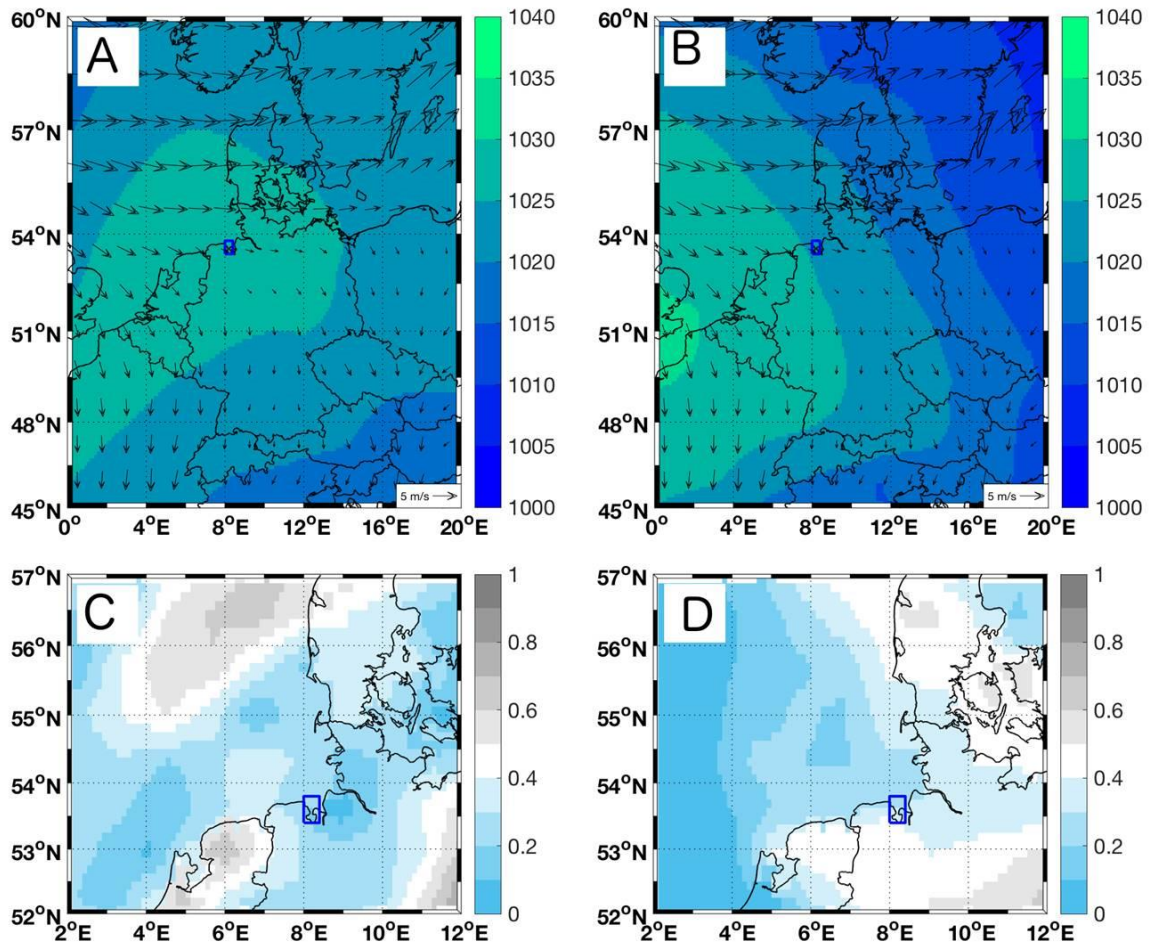


Figure 3: Mean Sea Level pressure (hPa) in blue to green contours and 10 m wind (black vector arrows) for Cycles 01 (A) and 03 (B). Low level cloud fraction for Cycles 01 (C) and 03 (D). All data was generated from average ERA-Interim (Dee et al. 2011). The location of Jade Bay is shown by the blue box.

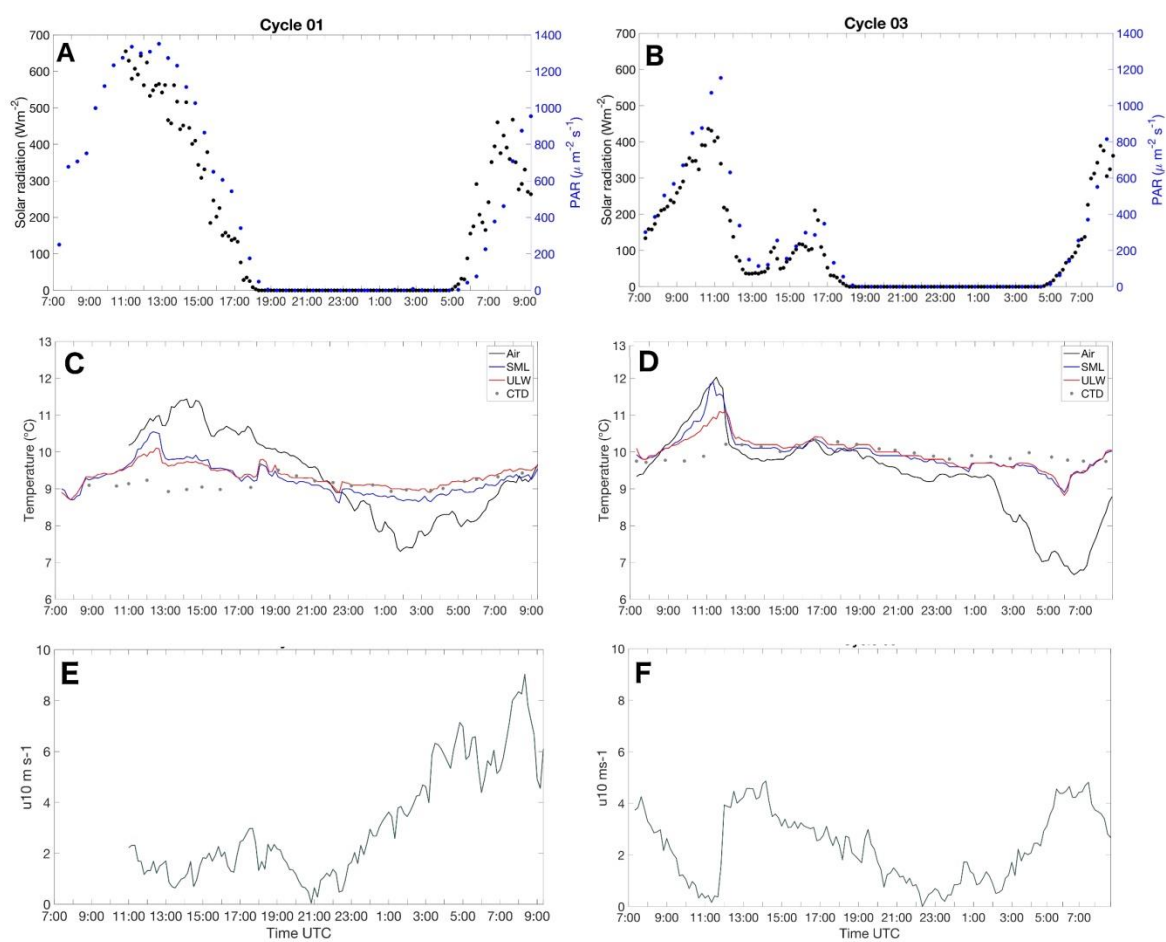


Figure 4: Solar Radiation (black circles) and photosynthetically active radiation (PAR; 410-655 nm, blue circles) for Cycles 01 (A) and 03 (B). Air temperature (black line), and water temperature in the sea surface microlayer (SML, blue line), underlying water (ULW, red line) and surface layer CTD (grey circles) for Cycles 01 (C) and 03 (D). Wind speed for Cycles 01 (E) and 03 (F) measured at the land-based weather station.

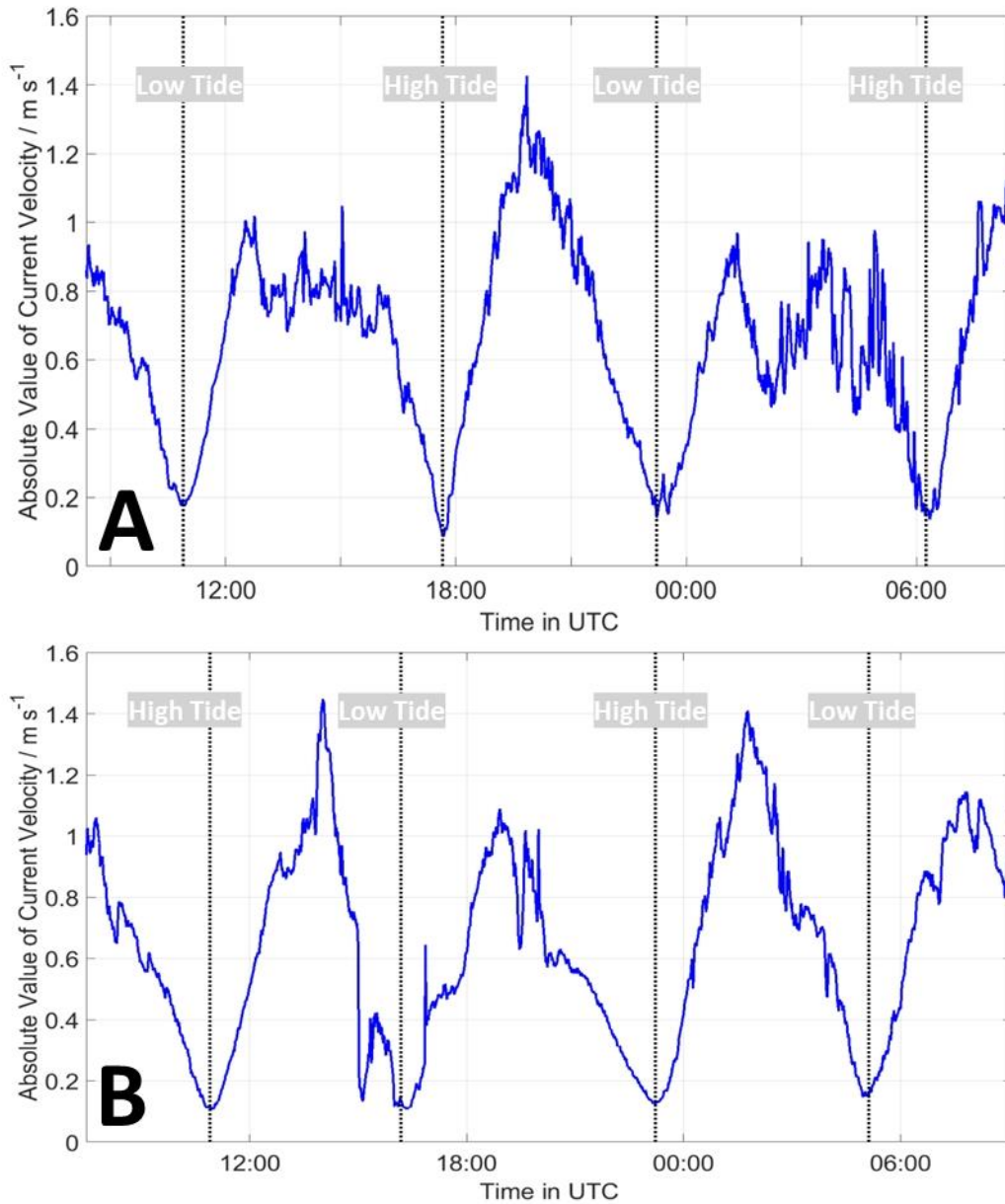


Figure 5: Current velocities measured during Cycle 01 (A) and Cycle 03 (B). Data were recorded in 3.6 to 4.6 m water depth (Cycle 01) and 1.7 to 2.7 m water depth (Cycle 03).

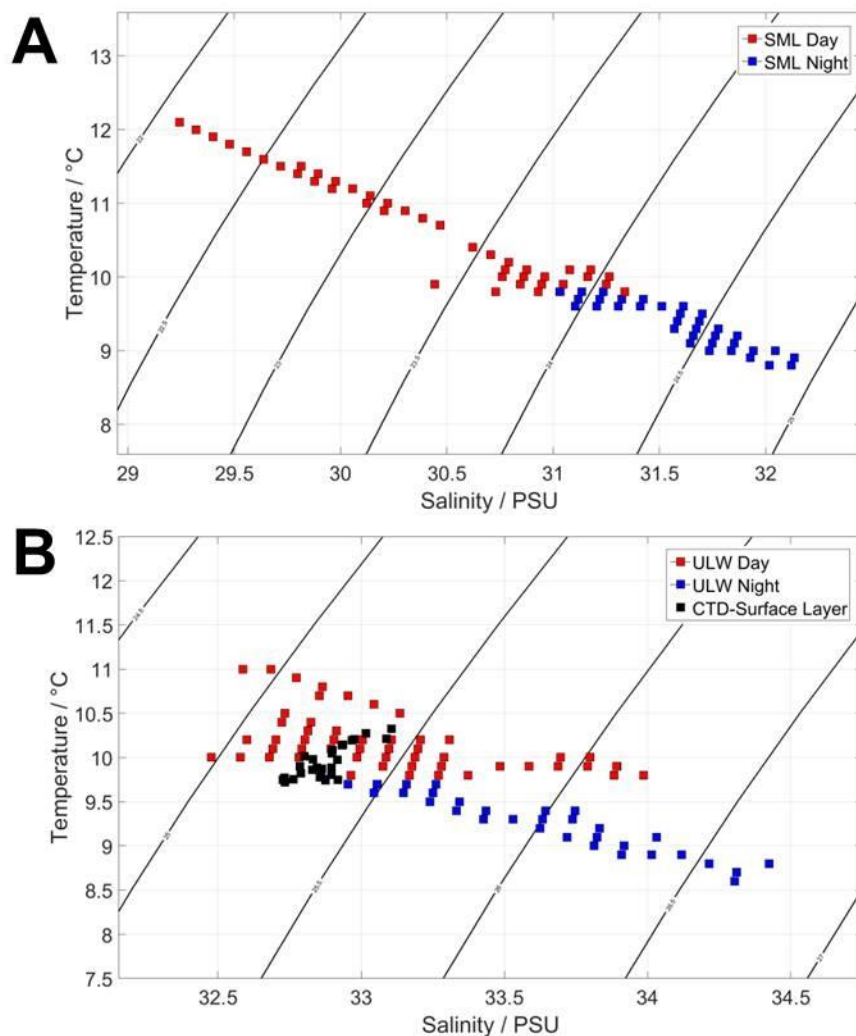


Figure 6: Temperature-salinity (T - S) diagram of (A) the sea surface microlayer (SML) and (B) the underlying water (ULW) and at the surface layer CTD (1.3 to 2 m depth) during Cycle 03. Day and Night measurements for SML and ULW are shown in red and blue color, respectively.

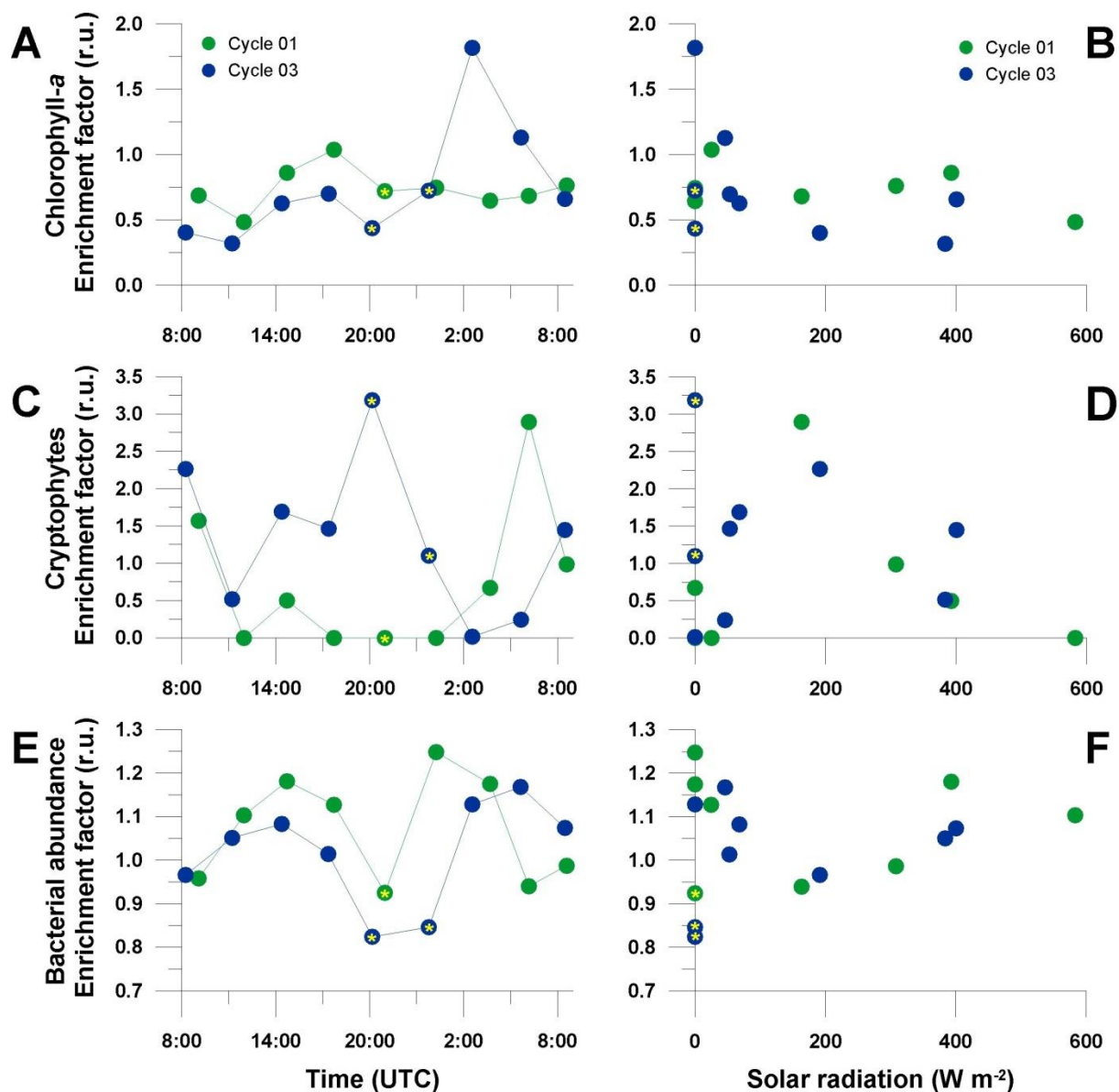


Figure 7: Biological parameters including Chlorophyll-a (A, B), the relative abundance of the phytoplankton group Chryptophytes (C,D), and bacterial abundance (E, F) during Cycles 01 (green) and 03 (blue). Results are shown as enrichment factor (relative concentration of a parameter x in the sea surface microlayer (SML) vs underlying water (ULW), i.e. $EF = SML[x] / ULW [x]$). EFs are plotted over time (A, C, E) and against solar radiation (B, D, F). Night samples taken at very low wind speed ($\leq 1 \text{ m s}^{-1}$) are marked (yellow asterisk).

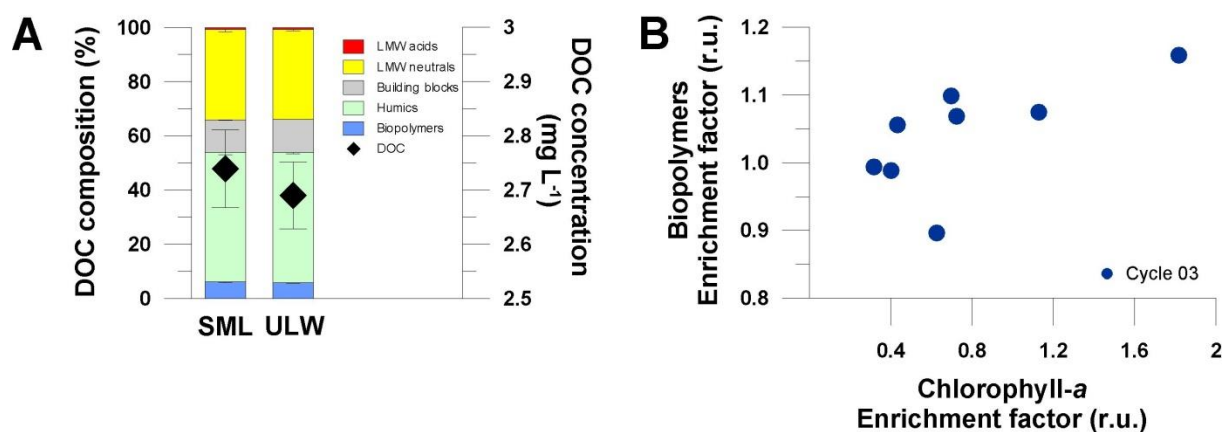


Figure 8: (A) Dissolved organic matter (DOM) composition of the different fractions identified in samples from the sea surface microlayer (SML) and underlying water (ULW) from Cycle 03. Additionally, dissolved organic carbon (DOC) concentration is shown as black diamonds. Error bars show standard deviation ($n = 9$) (B) The enrichment factor of the DOM fraction 'biopolymers' (i.e. $EF = \text{SML}[\text{biopolymers}] / \text{ULW}[\text{biopolymers}]$) is plotted against Chlorophyll-a.

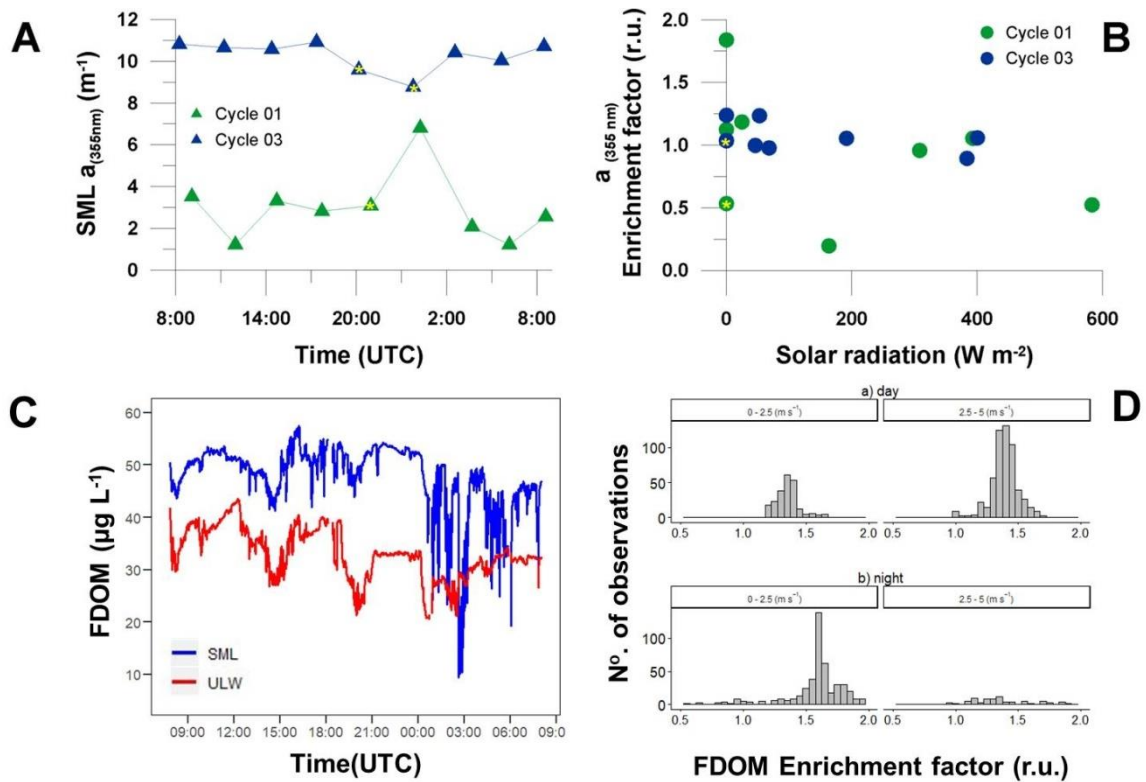


Figure 9: (A) Absorption coefficient (m⁻¹) of CDOM at 355 nm wavelength (λ) in sea surface microlayer (SML) samples during Cycle 01 (green) and Cycle 03 (blue). (B) Enrichment factor of $a_{355\text{ nm}}$ (i.e. $EF = SML[a_{355\text{ nm}}] / \text{underlying water (ULW)}[(a_{355\text{ nm}})]$) against solar radiation. Night samples taken at very low wind speed ($\leq 1\text{ m s}^{-1}$) are marked (yellow asterisk). (C) High resolution (0.1 Hz) of in-situ fDOM in the SML and ULW, and (D) histogram of enrichment factor (EF) of fDOM in the SML during day and night at different wind regimes.

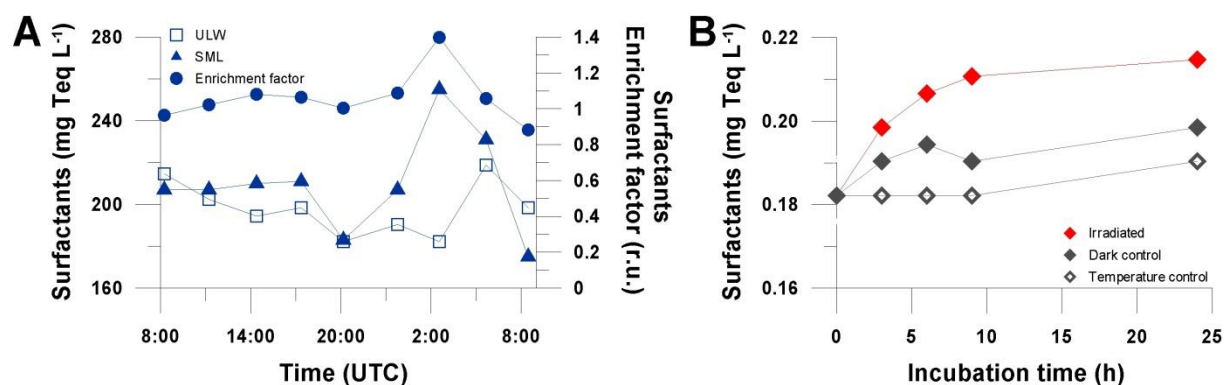


Figure 10: (A) Variability of surfactant concentration in the sea surface microlayer (SML, triangles) and underlying water (ULW, squares), and enrichment factors (EF, circles) during Cycle 03. (B) Changes in SML surfactant concentration during irradiance (red diamonds) compared to dark (black diamonds) and temperature controls (open diamonds) in the solar simulator.

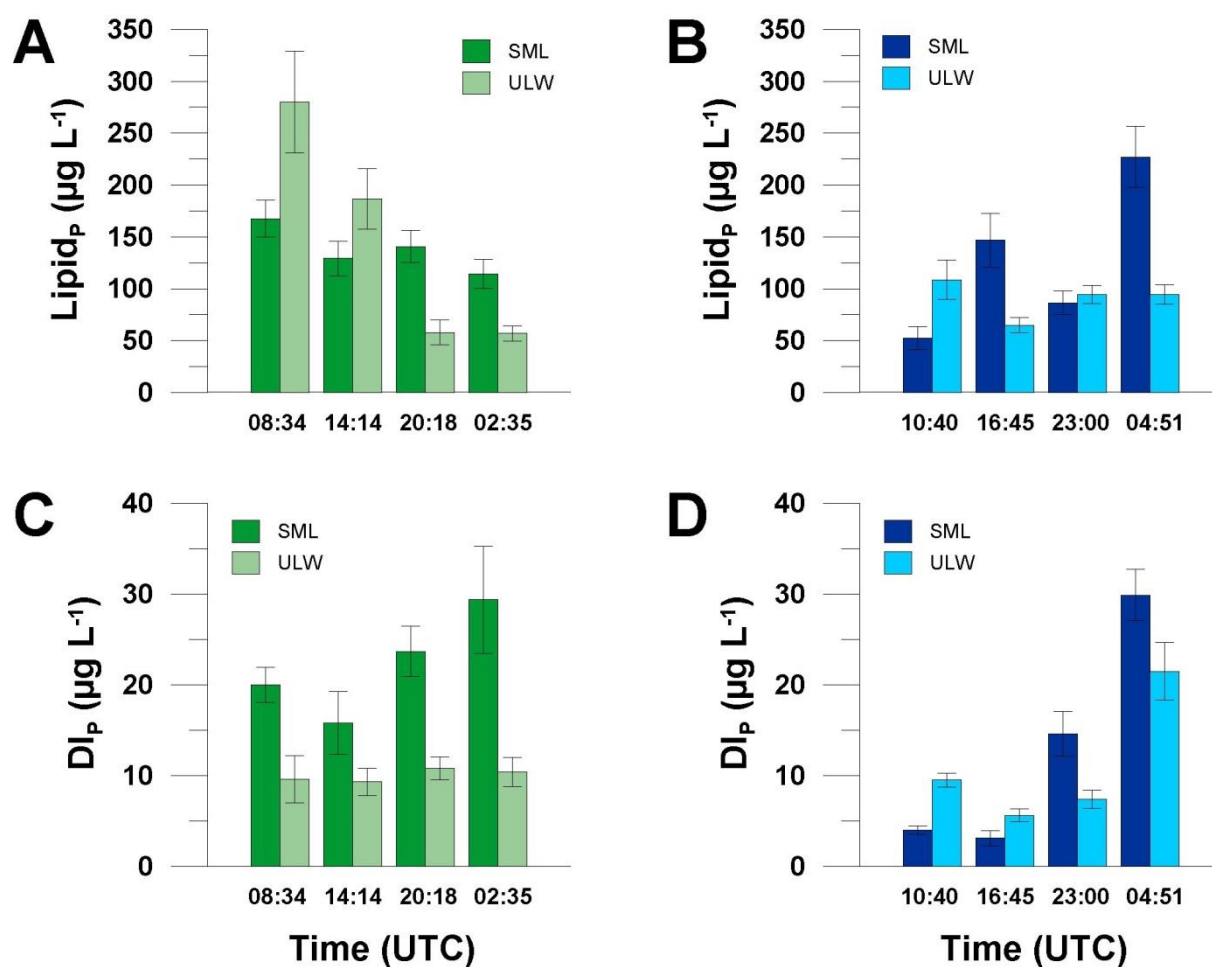


Figure 11: Concentrations of particulate lipids (A, B) and their degradation index (C, D) of some sea surface microlayer (SML) and underlying water (ULW) samples taken during Cycle 01 (green) and 03 (blue). Error bars show standard deviation of duplicate measurements.

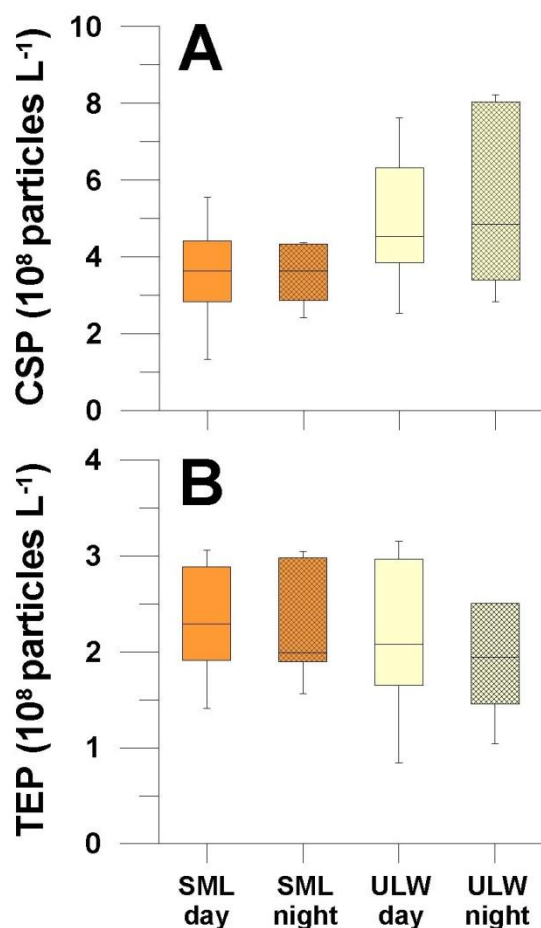


Figure 12: Box-whisker plot of the abundance of (A) Coomassie Stainable Particles (CSP) and (B) Transparent Exopolymer Particles (TEP) of sea surface microlayer (SML) and underlying water (ULW) samples taken during day and night. Combined data of Cycle 01 and 03 is shown. The boxes show the median (line) and the range of data from 25th and 75th percentiles ($n = 8-10$).

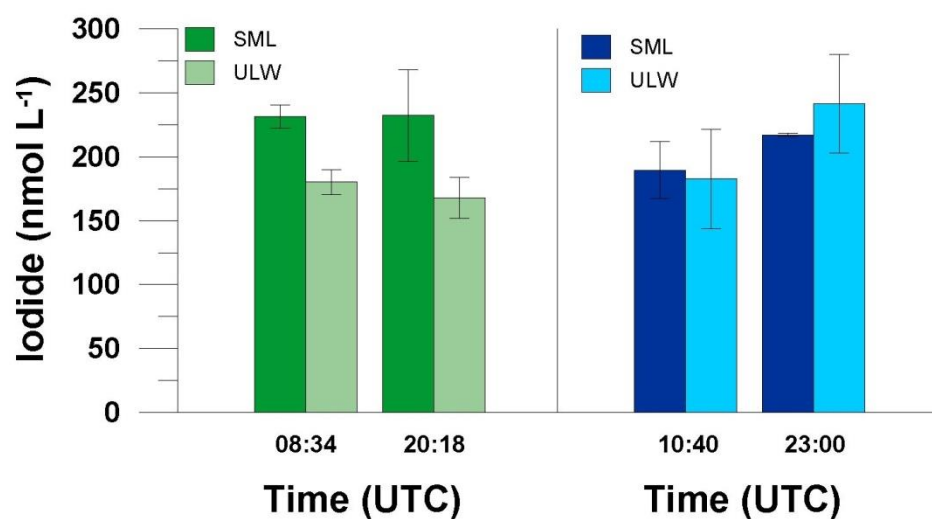


Figure 13: Iodide concentrations in filtered underlying water (ULW) and sea surface microlayer (SML) samples taken during Cycle 01 (green) and Cycle 03 (blue). Error bars show range (where $n=2$) or standard deviation (where $n>2$) of replicate measurements.

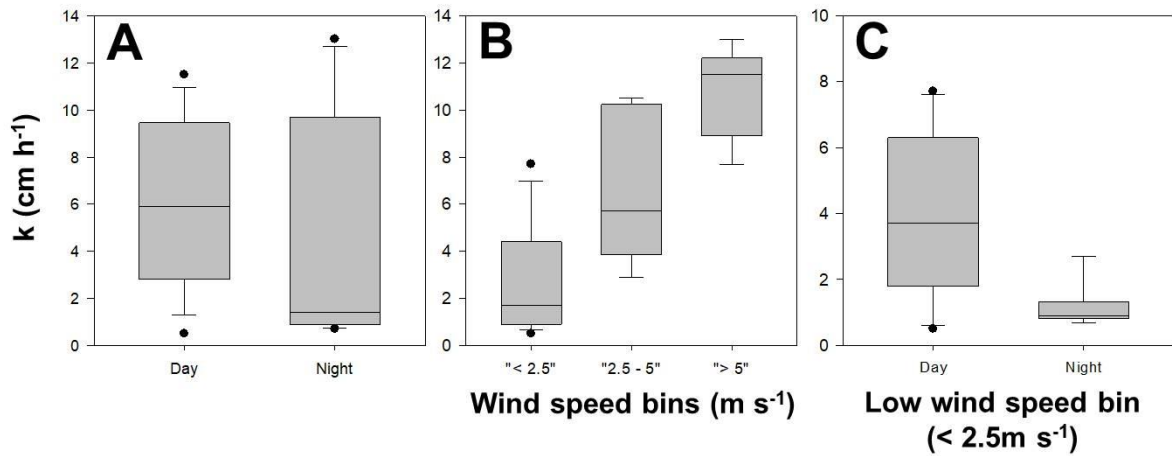
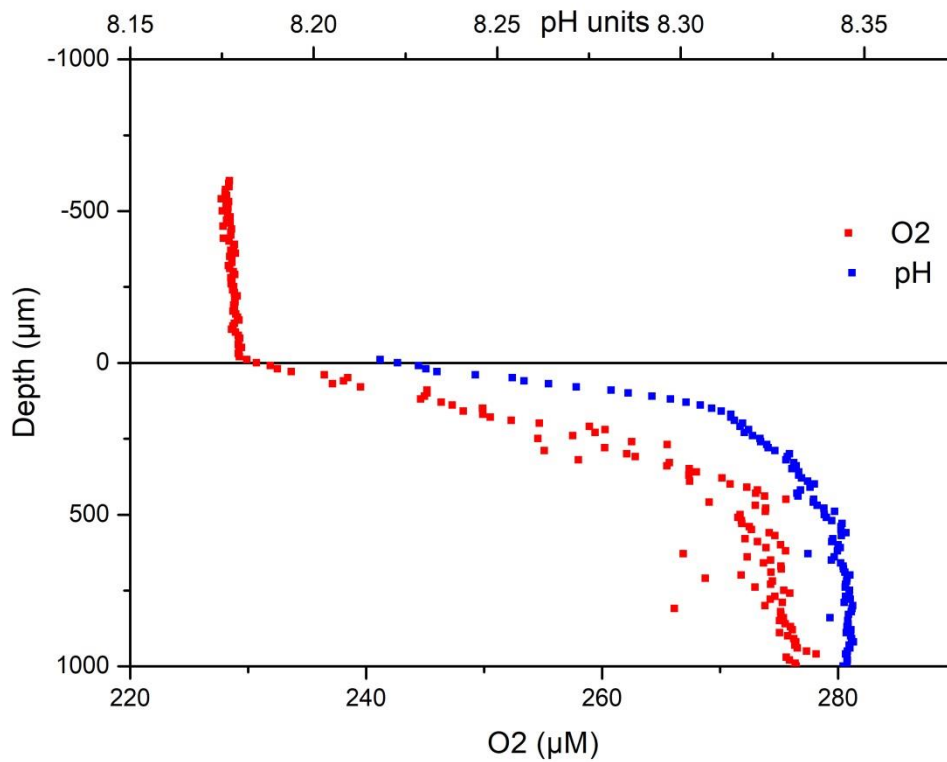


Figure 14: Box-whisker plots of the gas transfer velocities k for (A) day and night; (B) different wind speed bins; and (C) day and night for the low wind speed bin ($< 2.5 \text{ m s}^{-1}$). The boxes show the median (line) and the range of data from 25th and 75th percentiles; whiskers represent the 5th and 95th percentiles.



1010

1011 **Figure 15:** *Example gradients of oxygen (red) and pH (blue) across the air-sea interface*
 1012 *measured with microsensors in an aquarium filled with Jade Bay water.*

1013

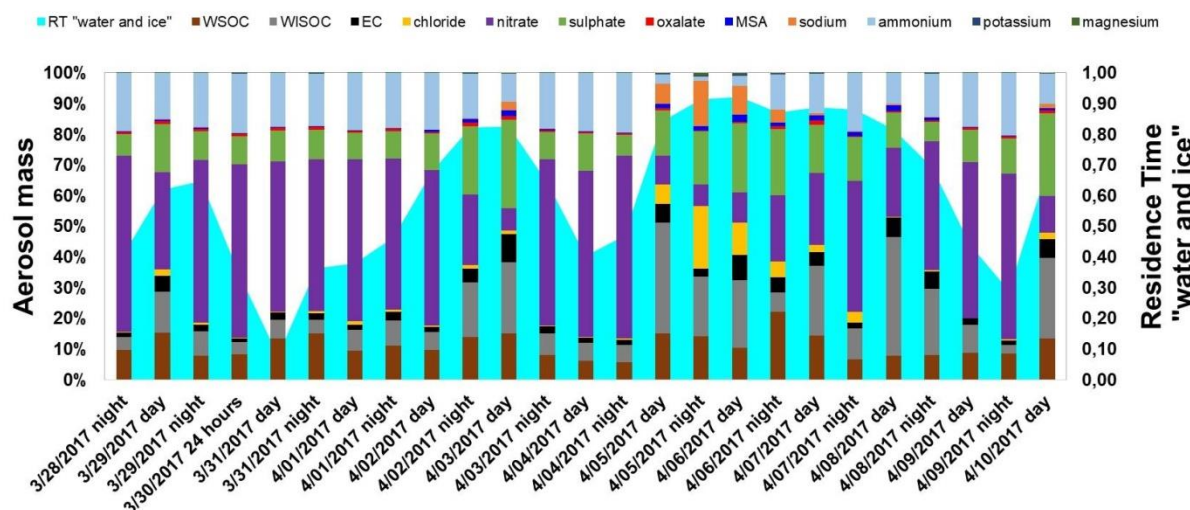


Figure 16: The respective contribution of different chemical species to the composition of the PM_1 aerosol particles including the main inorganic ions as well as organic carbon differentiated between water soluble organic carbon (WSOC) and water-insoluble organic carbon (WISOC). The residence time of the air masses over water and ice (RT "water and ice") is also shown.